COUPLED ANALYSIS OF THE MOTION AND MOORING LOADS OF A SPAR

'CONSTITUTION'

A Thesis

by

CHENGXI LI

Coupled Analysis of the Motion and Mooring Loads of A Spar 'CONSTITUTION'

COUPLED ANALYSIS OF THE MOTION AND MOORING LOADS OF A SPAR

'CONSTITUTION'

A Thesis

by

CHENGXI LI

Submitted to the Office of Graduate Studies of
Texas A&M University
in partial fulfillment of the requirements for the degree of

MASTER OF SCIENCE

Approved by:

Chair of Committee,   Jun Zhang
Committee Members,   Moohyun Kim
    David A. Brooks
Head of Department,   John Niedzwecki

August 2012

Major Subject: Ocean Engineering

ABSTRACT

Coupled Analysis of the Motion and Mooring Loads of A Spar

"CONSTITUTION". (August 2012)

Chengxi Li, B.E., Tianjin University

Chair of Advisory Committee: Dr. Jun Zhang

A truss spar, named as 'Constitution' was installed in Gulf of Mexico located at 90°58' 4.8" West Longitude and 27°17'31.9" North Latitude. Since its installation in October 2006, it has weathered multiple hurricanes. After the installation, British Maritime Technology (BMT) installed an Environmental Platform Response Monitoring System (EPRMS). The EPRMS is an integrated system collecting myriad of data that include the significant wave height and peak period of waves, the magnitude and direction of current and wind in the vicinity of the truss spar, its six-degree of freedom (6-D) motions, and tensions in its mooring lines and Top-Tension Risers. With the permission from Anadarko Petroleum Corporation (APC), these data are available to the Ocean Engineering Program at Texas A&M University (TAMU).

In this study, the coupled dynamic analysis of the spar interacting with the mooring and riser systems will be performed using a numerical code, named as 'COUPLE'. 'COUPLE' was developed and is continuously expanded and improved by his former and current graduate students and Professor Jun Zhang at TAMU for the computation of the

interaction between a floating structure and its mooring line/riser/tendon system in time domain. The main purpose of this study is to exam the accuracy and efficiency of 'COUPLE' in computing offshore structure motions and mooring line tensions and discuss the main issues of the computation. The numerical results will be compared with the corresponding ones obtained using another commercial software, 'Orcaflex', and the corresponding field measurement during Hurricane Ike which occurred on 12th September of 2008 and a winter storm on 9th November of 2009.

The satisfactory agreement between the numerical prediction made using 'COUPLE' and field measurement are observed and presented. The results of the comparisons between 'COUPLE' with 'Orcaflex' and field measurements in this study have verified the accuracy and efficiency of 'COUPLE' in computing offshore structure motions and mooring line tensions due to its nonlinear hybrid wave model which could better estimate the second-order difference-frequency wave loading.

ACKNOWLEDGEMENTS

TABLE OF CONTENTS

LIST OF FIGURES

LIST OF TABLES

1   INTRODUCTION

1.1   Overview

As the rapidly increasing demand of oil and gas, floating structures have been widely used for oil and gas production in deep water. Spar platform is one of such offshore floating structures used for deep water applications including the drilling, production, processing, and storage of the petroleum and natural gas. In Gulf of Mexico where oil storage is seldom a requirement, truss spars are the most widely used spars. According to the data from Bureau of Ocean Energy Management, Regulation and Enforcement (BOEMRE), so far there have been 17 spars in operation in Gulf of Mexico, including 3 classic spars, 13 truss spars and 1 cell spar (BOEMRE 2011).

The advantages of the truss spar over the Classic spar are: reduction in the total weight of the hull and fabrication costs, easy to fabricate, reduced drag loads leading to smaller surge offset in a high current environment and reduced loads on the mooring lines, heave plates reduced the heave motion of a truss spar leading to reduced fatigue loads on the risers, reduced draft allows shallower water applications, better VIV performance as the truss section is transparent to current, easy to be transported and flexibility in the installation of steel catenary risers (SCR) as truss section allowing to carry the risers through the sides of the spar (Theckumpurath 2006; Magee et al. 2000).

The Anadarko 'Constitution' platform is a truss spar platform which was installed in October of 2006 at 90°58'4.8" W, 27°17'31.9" N. The 'Constitution' is equipped with an

_____

This thesis follows the style of Journal of Ocean Engineering.

Environmental Platform Response Monitoring System (EPRMS), which records real-time motions, met-ocean conditions, mooring and riser loads. A detailed description of this type of monitoring system can be found in Prislin et al. (2005). These field measurements provide a great opportunity for calibrating and examining the numerical study of the six DOF motions, mooring line loads of the spar platform, which are very critical for design and sizing of the platform.

1.2 Background

1.2.1 Characteristics of "Constitution" Truss Spar

'Constitution' consists of four major components: topsides, hull, moorings and risers. The hull consists of three main parts: hard tank, truss and soft tank, each has the length of 74 m, 81m and 14 m, respectively (see Fig 1.1). The truss section is divided into four parts by three heave plates. See Table 1.1 for the main particulars of the 'Constitution'.

Table 1.1 Main particulars of the platform

Properties	Units	Value
Water Depth	m	1524
Draft	m	154
Center of Buoyancy from Keel	m	112.34
Center of Gravity from Keel	m	91.27
Topside Payload	ton	10770
Hull Weights	ton	14800
Total Displacement	ton	59250
Hard Tank Diameter	m	30
Length Overall	m	169
Hard Tank Length	m	74
Soft Tank Length	m	14
Truss Length	m	81
Truss Spacing	m	20
Fairlead Location from Keel	m	98
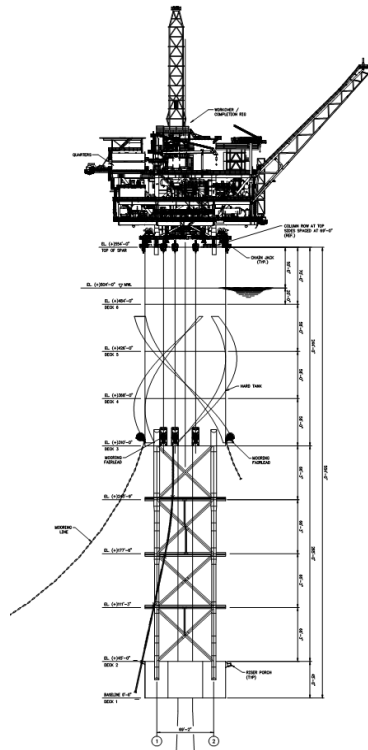
Fig. 1.1 Constitution spar elevation

1.2.2 The Mooring/Riser System

The mooring system of 'Constitution' consists of three groups and each group has three mooring lines. Each mooring line consists of three segments: platform chain, mid-section cable, and ground chain. The mooring line fairleads are located at the hard tank section, about 56 m below the sea surface. In addition, 'Constitution' has eight risers, six of which are production top tensioned risers (TTR) and two SCR. The detail mooring line and SCR particulars are listed in Table 1.2 and Table 1.3. Their arrangements and configurations are illustrated in Fig. 1.2 and Fig. 1.3 as well. Because the configuration data of the TTR is not available to us, the effect of TTR was simulated as a steady force in the heave direction, which was estimated based on the field measurement TTR tension data.

Table 1.2 Mooring line parameters.

	Platform chain	Mid-section	Ground Chain	Units
Line Type	R4 Studless	Steel Wire	R4 Studless	
Equivalent Diameter	0.142	0.127	0.142	m
Jacket Thickness	-	0.011	-	m
Weight in Air	403	84	403	kg/m
Weight in Water	351	66	351	kg/m
EA	152,957	151,020	152,957	ton
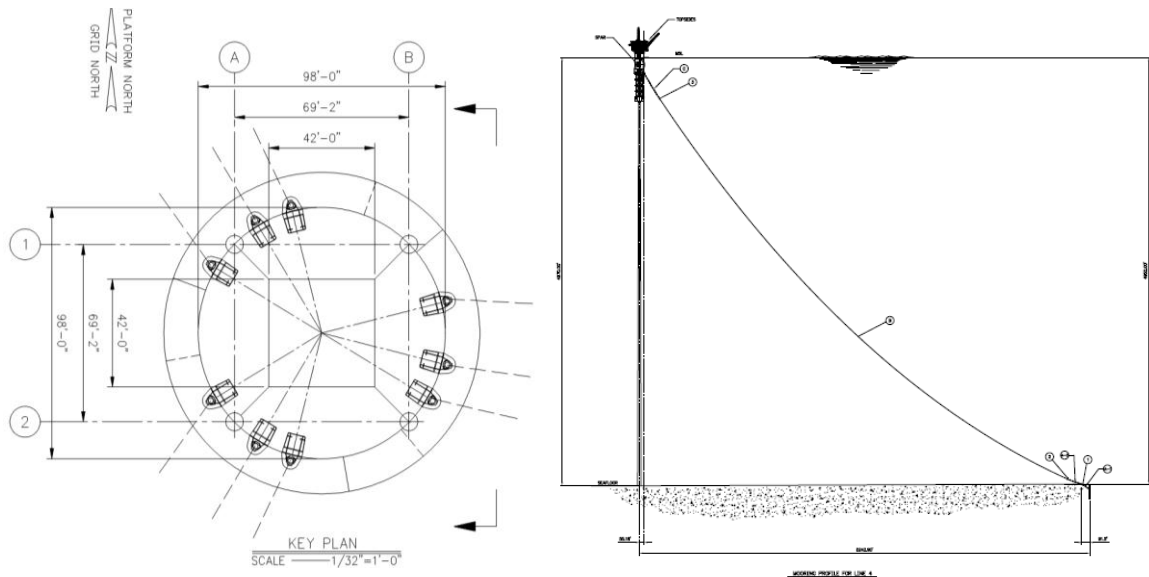
Fig. 1.2 Mooring line arrangement and configuration.

Table 1.3 SCR parameters.

	SCR 1	SCR 2	Units
Length	1706.88	1706.88	m
Diameter	0.254	0.3048	m
Dry Weight	57.3	97.8	kg/m
Unit Buoyancy	52.19	75.15	kg/m
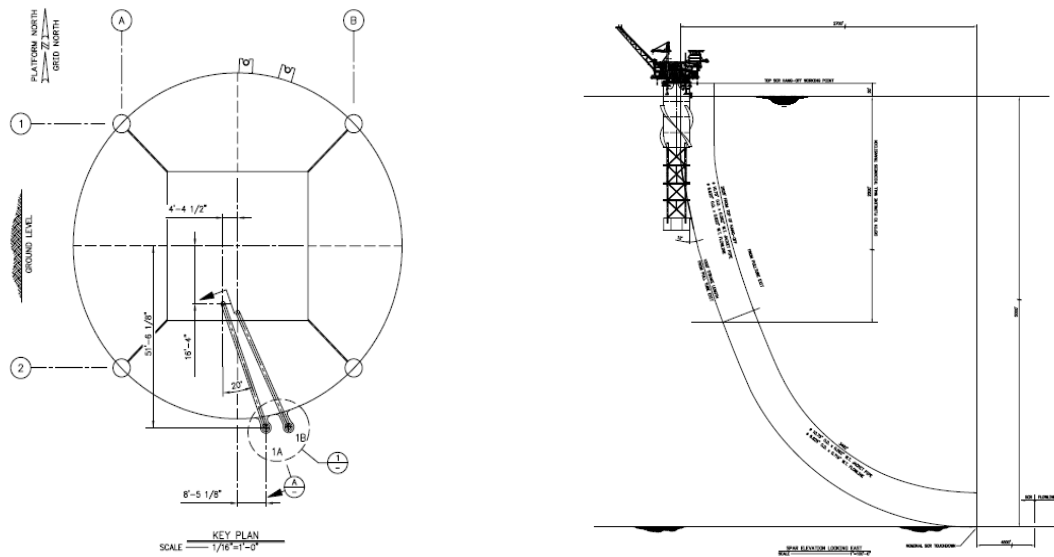
Fig. 1.3 SCR arrangement and configuration.

1.3   Review of Previous Study

An integrated floating structure consists of a mooring/riser system and a moored floating structure (hull). Coupled dynamic analysis considers the interactions between these two components in calculating the motions and forces of a floating structure.

Many studies using the coupled analysis were carried out on Spars, Semi-submersibles and FPSOs (Ran and Kim 1997; Ran et al. 1998; Ormberg and Larsen 1997; Ormberg et al. 1998; Ma et al. 2000). In these studies, the coupling effects between a moored structure and its mooring system in general followed the same procedure. The hydrodynamic coefficients were first calculated in the frequency domain numerical software or based on empirical data. Based on the wave force RAO and quadratic transfer functions, the wave forces on the structure were then computed in time domain using the inverse Fast Fourier Transform (I/FFT) technique (Yang et al. 2011). The dynamic

analysis of a mooring system was conducted in time domain using a code based on either Finite Element Method (FEM) or lumped-mass method.

A simplified alternative was developed to compute the wave loading based on the slender-body approximation (Kim and Chen 1994), that is, without explicitly consider the diffraction and radiation effect due to the presence of the structure. For a typical deep-water offshore structure such as the 'Constitution' in this case, the ratio of the structure dimension to the characteristic design wavelength is usually small (less than 0.2). Hence it may be assumed that the wave field is not disturbed by the structure and that the modified Morison equation (Morison et al., 1950) is adequate to calculate the first and second-order wave exciting forces (Cao and Zhang 1997). Paulling and Webster (1986) used the Morison Equation in a coupled dynamic analysis of a TLP. Cao and Zhang (1997) used the Morison Equation with a unidirectional Hybrid Wave Model (HWM) in the coupled analysis of a JIP Spar. Also Kim and Chen (1994) compared the second-order diffraction/radiation theory with slender body approximation (modified Morison equation) in the frequency domain for an Articulated Loading Platform (ALP).

In recent years, Kim et al. (2005) used the coupled dynamic analysis program for the global motion simulation of a turret-moored, tanker based FPSO designed for 6000-ft water depth. Chen et al. (2006) compared the numerical results with experiment measurements for a mini TLP.

The comparison between the field measurement data and the numerical simulated results was also carried out by many other studies such as the numerical study of the 6

DOF motions of 'Horn Mountain' spar (Theckumpurath, 2006) and the numerical studies of the spar field mooring line tensions (Tahar et al. 2005; Kieke and Zhang 2012).

In this study, the author focuses on the mooring line cable dynamic analysis and couple dynamic analysis of the spar motions. A coupled dynamic analysis program called 'COUPLE', which is applicable to Spars and TLPs, has been used and compared not only with the field data measurement but also the numerical results from 'Orcaflex', which is widely used in the industry. The differences among the numerical results and field data were compared and analyzed.

1.4   Objective

The field measurement data was collected by the EPRMS installed on 'Constitution' spar, which is deployed in water depth of 1524 m and has nearly 154 m structure height. A numerical code 'COUPLE' is used to simulate the platform structure and calculate the coupled dynamic results during different ocean environment conditions. These results will then be compared with the field measurement data as well as the numerical results obtained from a commercial software, 'Orcaflex'.

In this study, the author presents the numerical results of the spar motion and mooring tension loads under the impact of hurricane Ike which occurred on 12th September of 2008 and a winter storm which occurred on 9th November of 2009. This study discusses the main issues for computing the global performance response and mooring analysis of a truss spar in deep water such as the validation of using the Morison equation in calculating the wave loads. It also examines the spar structure's motion under the hurricane environment and its interaction with its mooring systems. Various major parameters of the

spar platform are derived such as the spar wind coefficient, drag and added-mass coefficients of the heave plates, hard tank and truss beams. The comparison between numerical results and the field measurements exams the accuracy and efficacy of numerical codes 'COUPLE' and 'Orcaflex' in the computation of the offshore structure motion and mooring line tension. The numerical results based on different wave models are also compared in order to exam their accuracy, such as linear extrapolation, wheeler stretching and hybrid wave model (HWM).

The dynamic of mooring lines and risers are calculated using a module included in 'COUPLE', named as 'CABLE3D'. This module was developed for the dynamic analysis of the mooring/riser/tendon system based on a Finite Element Method and slender-body assumption (Garrett 1982).

2   METHODOLOGY

2.1   Numerical Simulation

For the global performance analysis of 'Constitution', an in-house numerical code 'COUPLE' and the commercial software 'Orcaflex' were used. Comprehensive comparison among the prediction from 'COUPLE', 'Orcaflex' and the field measurement data were made to verify the accuracy and efficacy of both the codes. The theories of the calculation are briefly described in this chapter.

2.1.1   COUPLE

The numerical code, known as COUPLE, was developed and is continuously expanded and improved by his former and current graduate students and Professor Jun Zhang at Texas A&M University for the computation of the interaction between a floating structure and its mooring line/riser/tendon system in time domain.

The hydrodynamic forces applied on the spar are computed by the Morison equation. An implied assumption for Morison equation is that the wavelength is long compared to the member's cross sectional dimensions. This assumption can be satisfied since 'Constitution' spar platform can be considered as a slender body comparing with the large wavelength during the hurricane in the Gulf of Mexico. The spar motion is computed under the theory of 6-DOF nonlinear motion equations of a rigid body. Then the motion equations of a rigid body are coupled to dynamic equations of slender rods, which are used to calculate the interactions of the mooring/riser system, through hinged boundary conditions to get the coupled dynamic numerical results of the platform. The theories of

the numerical code 'COUPLE' were detailed described in Chen et al. (2006) and introduced below for completeness.

2.1.1.1 6-DOF Nonlinear Motion Equations of a Rigid Body

For a single module, two coordinate systems are defined and shown in Fig. 2.1. System *OXYZ* is assumed fixed in the body and, for convenience, its origin can be located at the center of gravity. The *XY*-plane is parallel to the water surface when the body floats at rest in calm water and *OZ* is directed vertically upward. The second coordinate system, $\hat{o}\hat{x}\hat{y}\hat{z}$, is fixed in space at the initial position of *OXYZ*, forming space-fixed coordinate system. The equations of motion for the body express the position and motion of *OXYZ* with respect to $\hat{o}\hat{x}\hat{y}\hat{z}$ in terms of the body properties and the external forces such as those caused by waves, interaction with mooring/riser system.
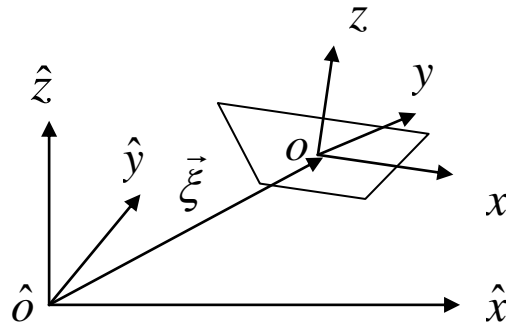
Fig. 2.1 Global and body coordinate.

The derivation of the equations of motion for a single rigid body having six degrees of motion freedom may be found in standard dynamics textbooks. The result will be presented below:

The translational motion equations of a rigid body expressed in the $\hat{o}\hat{x}\hat{y}\hat{z}$ (spaced-fixed) coordinate system and the rotational motion equations expressed in the $oxyz$ (body-fixed) coordinate system with respect to o are:

$$m\frac{d^2\boldsymbol{\xi}}{dt^2} + m\mathbf{T}^t(\frac{d\boldsymbol{\omega}}{dt}\times\mathbf{r}_g) + m\mathbf{T}^t(\boldsymbol{\omega}\times(\boldsymbol{\omega}\times\mathbf{r}_g)) = \hat{\mathbf{F}} \qquad (2.1)$$

$$\mathbf{I}_o\frac{d\boldsymbol{\omega}}{dt} + \boldsymbol{\omega}\times\mathbf{I}_o\boldsymbol{\omega} + m\mathbf{r}_g\times(\mathbf{T}\frac{d^2\boldsymbol{\xi}}{dt^2}) = \mathbf{M}_o \qquad (2.2)$$

where:

superscript t represents transpose of a matrix;

$\hat{\mathbf{a}}_o = \dfrac{d^2\boldsymbol{\xi}}{dt^2}$, is the acceleration at point o of the body expressed in $\hat{o}\hat{x}\hat{y}\hat{z}$;

$\boldsymbol{\xi} = (\xi_1,\ \xi_2,\ \xi_3)^t$, is the displacement at point o of the body expressed in $\hat{o}\hat{x}\hat{y}\hat{z}$;

$\boldsymbol{\omega} = (\omega_1, \omega_2, \omega_3)^t$, is the angular velocity expressed in $oxyz$;

$\mathbf{r}_g = (x_g, y_g, z_g)^t$, is the vector of the center of gravity of the body expressed in $oxyz$;

$\mathbf{I}_o$ is the moment of inertia of the body with respect to o expressed in $oxyz$;

$\hat{\mathbf{F}}$ is the total forces applied on the body expressed in $\hat{o}\hat{x}\hat{y}\hat{z}$;

$\mathbf{M}_o$ is the total moments with respect to o the origin of the $oxyz$ coordinates;

$\mathbf{T}$ is a transfer matrix between the body-fixed coordinate system and the space-fixed coordinate system expressed as:

$$\mathbf{T} = \begin{bmatrix} \cos\alpha_3\cos\alpha_2 & \sin\alpha_3\cos\alpha_1 + \cos\alpha_3\sin\alpha_2\sin\alpha_1 & \sin\alpha_3\sin\alpha_1 - \cos\alpha_3\sin\alpha_2\cos\alpha_1 \\ -\sin\alpha_3\cos\alpha_2 & \cos\alpha_3\cos\alpha_1 - \sin\alpha_3\sin\alpha_2\sin\alpha_1 & \cos\alpha_3\sin\alpha_1 + \sin\alpha_3\sin\alpha_2\cos\alpha_1 \\ \sin\alpha_2 & -\cos\alpha_2\sin\alpha_1 & \cos\alpha_2\cos\alpha_1 \end{bmatrix} \quad (2.3)$$

$\mathbf{T}$ is an orthogonal matrix with the property that $\mathbf{T}^t = \mathbf{T}^{-1}$.

The relationship between space-fixed coordinates $\hat{\mathbf{x}} = (\hat{x}, \hat{y}, \hat{z})^t$ and body-fixed coordinates $\mathbf{x} = (x, y, z)^t$ is:

$$\hat{\mathbf{x}} = \boldsymbol{\xi} + \mathbf{T}^t\mathbf{x} \qquad (2.4)$$

2.1.2   Mooring Line and Riser Simulation

Mooring lines and risers were modeled using a module included in 'COUPLE', which is named as 'CABLE3D'. This module was developed for the dynamic analysis of the mooring/riser/tendon system with Finite Element Method and slender-body assumption (Garrett 1982). The current load and VIV effects were also involved in 'COUPLE' (Ding et al. 2003) and this study. Recently, it also takes into account for the interaction between a riser and its anchor's foundation.

In the 'CABLE3D', mooring lines and risers are regarded as a long slender structure with negligible moments and shear forces. Derivations of equations of motion of a slender rod summarized below, mainly follows the work by Love (1944), Nordgren (1974), Garrett (1982), Paulling and Webster (1986), and Ma and Webster (1994).

The internal state of stress at a point on the rod is described fully by the resultant force $\mathbf{F}$ and the resultant moment $\widetilde{\mathbf{M}}$ acting at the centerline of the rod. We can derive the following equations on the basis of the momentum conservation:

$$\mathbf{F}' + \mathbf{q} = \rho\ddot{\mathbf{r}}(s,t) \tag{2.5}$$

$$\widetilde{\mathbf{M}}' + \mathbf{r}' \times \mathbf{F} + \mathbf{m} = 0 \tag{2.6}$$

where $\mathbf{q}$ is the distributed external force per unit length, ρ is the mass per unit length, $\mathbf{m}$ is the external moment per unit length, and a superposed dot denotes differentiation with respect to time. The prime denotes the derivatives with respect to s. In above equations, the effects of rotary inertia and shear deformations are neglected.

For a elastic rod with equal principal stiffness, the resultant moment $\widetilde{\mathbf{M}}$ can be written as:

$$\widetilde{\mathbf{M}} = \mathbf{r}' \times (B\mathbf{r}'') + H\mathbf{r}' \tag{2.7}$$

$$\widetilde{\mathbf{M}}' = \mathbf{r}' \times (B\mathbf{r}'')' + H'\mathbf{r}' + H\mathbf{r}'' \tag{2.8}$$

where H is the torque and B is the bending rigidity. Assuming $H=0$ and $\mathbf{m}=0$, and plug $\widetilde{\mathbf{M}}'$ into equation (2.6), equations (2.5) and (2.6) reduced to the expression of $\mathbf{F}$:

$$\mathbf{F} = \lambda\mathbf{r}' - (B\mathbf{r}'')' \tag{2.9}$$

$$\lambda = T - B\kappa^2 \tag{2.10}$$

where $\kappa^2 = -\mathbf{r}'\cdot\mathbf{r}'''$, κ is the local curvature of the rod, and $T(s,t) = \mathbf{r}'\cdot\mathbf{F}$ is the local tension. Because of the inextensibility assumption:

$$\mathbf{r}'\cdot\mathbf{r}' = 1 \tag{2.11}$$

The equation of motion is finally derived by plugging $\mathbf{F}$ of (2.9) into (2.5):

$$-(B\mathbf{r}'')'' + (\lambda\mathbf{r}')' + \mathbf{q} = \rho\ddot{\mathbf{r}} \tag{2.12}$$

$$\mathbf{r}'\cdot\mathbf{r}' = (1+\varepsilon)^2 \tag{2.13}$$

where $\varepsilon = \dfrac{T}{EA}$, EA is the elastic stiffness of the rod. When ε is very small, equation of

motion (2.13) and equation of Lagrange multiplier λ (2.10) are valid. $\mathbf{q}$ is external force

per unit length and $\rho = \rho_t A_t$ is mass per unit length.

The external forces applied on a rod consist of gravity forces, hydrostatic and

hydrodynamic forces. The gravity force on the rod leads to a distributed load given by:

$$\mathbf{q}_t(s,t) = -\rho_t g A_t \mathbf{e}_y \tag{2.14}$$

The hydrodynamic forces acting on the rod consist of added-mass force, drag force,

and Froude-Krylov force. The Morrison equation is used to predict the first two terms:

$$\mathbf{q}_f^I(s,t) = \rho_f A_f C_{Mn} \mathbf{N}(\mathbf{a}_f - \ddot{\mathbf{r}}) + \rho_f A_f C_{Mt} \mathbf{T}(\mathbf{a}_f - \ddot{\mathbf{r}}) \tag{2.15}$$

$$\begin{aligned}\mathbf{q}_f^D(s,t) &= \frac{1}{2}\rho_f D_f C_{Dn} \mathbf{N}(\mathbf{v}_f - \dot{\mathbf{r}})\left\|\mathbf{N}(\mathbf{v}_f - \dot{\mathbf{r}})\right\| \\ &+ \frac{1}{2}\rho_f D_f C_{Dt} \mathbf{T}(\mathbf{v}_f - \dot{\mathbf{r}})\left\|\mathbf{T}(\mathbf{v}_f - \dot{\mathbf{r}})\right\|\end{aligned} \tag{2.16}$$

where C_{Mn}, C_{Mt}, C_{Dn} and C_{Dt} are the normal added-mass coefficient, tangential added-mass

coefficient, normal drag coefficient and tangential drag coefficient respectively.

Froude - Krylov force due to sea water outside the rod is:

$$\mathbf{q}_f^{F-K}(s,t) = \rho_f(g\mathbf{e}_y + \mathbf{a}_f)A_f + (P_f A_f \mathbf{r}')' \tag{2.17}$$

Froude-Krylov force (pressure forces) due to the fluid inside the rod is:

$$\mathbf{q}_i^{F-K}(s,t) = -\rho_i g A_i \mathbf{e}_y - (P_i A_i \mathbf{r}')' \tag{2.18}$$

In the above equations:

$\rho = \rho_t A_t + \rho_i A_i$, the mass per unit rod (including the internal fluid),

$\rho_f(s)$ = the mass density of the sea water,

$\rho_i(s)$ = the mass density of the inside fluid,

$\rho_t(s)$ = the mass density of the tube,

$A_f(s)$ = the outer cross-section area of the rod,

$D_f(s)$ = the diameter of the rod,

$A_i(s)$ = the inner cross-section area of the rod,

$A_t(s)$ = the structural cross-section area of the rod,

$\mathbf{v}_f$ = the velocity of the sea water (current and wave),

$\mathbf{a}_f$ = the acceleration of the sea water (current and wave),

P_f = pressure of the sea water,

P_i = pressure of the internal fluid,

$\mathbf{T}, \mathbf{N}$ = transfer matrices,

$\mathbf{I}$ = identity matrix,

where the subscripts f, i and t denote the sea water, the fluid inside the tube and the tube itself. $\mathbf{T}$ and $\mathbf{N}$ are defined by:

$$\mathbf{T} = \mathbf{r}'^T \mathbf{r}' \tag{2.19}$$

$$\mathbf{N} = \mathbf{I} - \mathbf{T} \tag{2.20}$$

After expressing the external forces, the governing equation is derived:

$$\mathbf{M}\ddot{\mathbf{r}} + (B\mathbf{r}'')'' - (\tilde{\lambda}\mathbf{r}')' = \mathbf{q} \tag{2.21}$$

where

$$\mathbf{q} = (\rho_f A_f - \rho_t A_t) g \mathbf{e}_y + \rho_f A_f (1+\varepsilon)(\mathbf{I} + C_{Mn}\mathbf{N} + C_{Mt}\mathbf{T})\mathbf{a}_f$$

$$+ \frac{1}{2}\rho_f D_f C_{Dn}(1+\varepsilon)\mathbf{N}(\mathbf{v}_f - \dot{\mathbf{r}})|\mathbf{N}(\mathbf{v}_f - \dot{\mathbf{r}})| \qquad (2.22)$$

$$+ \frac{1}{2}\rho_f D_f C_{Dt}(1+\varepsilon)\mathbf{T}(\mathbf{v}_f - \dot{\mathbf{r}})|\mathbf{T}(\mathbf{v}_f - \dot{\mathbf{r}})|$$

$$\mathbf{M} = (\rho_t A_t + \rho_i A_i)\mathbf{I} + \rho_f A_f C_{Mn}\mathbf{N} + \rho_f A_f C_{Mt}\mathbf{T} \qquad (2.23)$$

$$\tilde{\lambda} = (T + P_f A_f - P_i A_i) - B\kappa^2$$

The procedures for numerical implementation for the equations above are the same as described in Garrett (1982). The Galerkin's method is adopted to discretize the partial differential equations of motion (2.12) and the constraints equations (2.13) in space by using different shape functions. The detailed procedure for this calculation can be found in Chen et al. 2006.

2.1.3 Coupled Dynamic Analysis

By applying the boundary conditions at fairleads, then motion equations of the hull and dynamic equations of the spar mooring/riser system are integrated.

Assume the fairlead is at $s = 0$, then the generalized forces and moments applied on at the fairlead of lth mooring line/riser is:

$$\mathbf{f}_1 = -\{\tilde{\lambda}\mathbf{r}'(0) - (B\mathbf{r}'')'(0)\} = -\mathbf{F}(0) \qquad (2.24)$$

$$\mathbf{f}_2 = -\frac{1}{L}B\mathbf{r}''(0) \qquad (2.25)$$

If the mooring/riser system consists of L individual mooring lines and risers, the mooring/riser system forces applied on the hull are the summation of forces and moments

of each mooring line/riser applied on the structure at the fairlead. The forces and moments of the mooring system applied on the hull can be expressed as:

$$\mathbf{F}_M = \sum_{l=1}^{L}(\mathbf{LF}_l) \tag{2.26}$$

$$\mathbf{M}_M = \sum_{l=1}^{L}\left[\mathbf{r}_{cl} \times (\mathbf{TLF}_l) + \mathbf{TL}\widetilde{\mathbf{M}}_l\right] \tag{2.27}$$

where $\mathbf{L}$ is a transfer matrix between the spaced-fixed coordinates for the mooring /tendon/riser system and the hull.

$$L = \begin{Bmatrix} 1 & 0 & 0 \\ 0 & 0 & -1 \\ 0 & 1 & 0 \end{Bmatrix} \tag{2.28}$$

It should be noted that $\mathbf{F}_M$ is expressed in the space-fixed coordinate system $\hat{o}\hat{x}\hat{y}\hat{z}$, and $\mathbf{M}_M$ is expressed in the body-fixed coordinate system $oxyz$. When hinged boundary conditions are applied, $\widetilde{\mathbf{M}}_l = 0$.

Finally, in order to solve the 6DOF motion equation in the time domain, the external forces and the coupled mooring forces are evaluated at each time step at the instantaneous body position and up to the free surface, and then the equation evolves to the next time step using a step-by-step numerical integration scheme. There are many integration methods available, such as Newmark-β, Wilson-θ and Runge-Kutta methods. Implicit Newmark-β method is used in 'COUPLE' as it is considered as suitable in solving nonlinear differential equations because of its high accuracy and numerical stability.

2.2   Wave Theory

The wave loads were computed using Morison Equation in the numerical models of this study (both 'COUPLE' and 'Orcaflex'). As a result, the wave kinematics solutions become very important in the calculation of the wave loads. Different wave theories were employed to calculate the wave kinematics for the numerical model such as: Wheeler stretching (WL) and linear extrapolation (LE) in 'Orcaflex' and Hybrid Wave Models (HWM) in 'COUPLE'. The detailed descriptions of these models are summarized below.

2.2.1   Modifications of Linear Wave Theory

The traditional modification methods of the linear wave theory used in 'Orcaflex' for computing the wave kinematics intend to correct the related prediction based on linear wave theory (LWT). LWT assumes that the wave heights are infinitesimal such that the shape of the instantaneous free surface and any water particle kinematic variable can be described by the superposition of various regular small amplitude waves. As should be expected, when wave height is large relative to the wavelength, linear theory provides unacceptable result near the free surface. Empirical modification of the results of LWT have been used to provide more accurate wave kinematics up to the instantaneous free surface near the wave crests, where LWT is weakest. The most widely used empirical models are known as stretching techniques. This technique has been briefly described in the forthcoming sub-sections (Rodenbusch and Forristall 1986).

2.2.1.1 Wheeler Stretching

Wheeler stretching maps the linear wave kinematics profile from sea bottom to mean water level (MWL) into the profile from sea bottom to instantaneous water surface through the vertical coordinate mapping.

$$z_w = \frac{d(d+z)}{d+\eta} - d \tag{2.29}$$

where z is the vertical coordinate, $-d < z < \eta$, d the water depth, η the instantaneous free surface elevation, and z_w denotes the transformed vertical coordinate to be entered in the result of the linear wave theory to obtain the modified kinematics at the real physical z. The profile of fluid kinematics obtained from LWT is stretched or compressed between sea bottom and the instantaneous free surface. In summary, the wave induced water particle velocities and accelerations calculated at the MWL using linear wave theory are equal to those at the free surface using wheeler stretching.

2.2.1.2 Linear Extrapolation

Linear extrapolation is made only in the region between the free surface above the MWL and the MWL, by replacing the wave kinematics in this region with a truncated Taylor's expansion for $z > 0$.

$$u(x,z,t) = u(x,0,t) + z\frac{\partial u}{\partial z}(x,0,t) \quad (0 < z < \eta) \tag{2.30}$$

However, studies show computations based on different modified linear models may give quite different predictions of wave kinematics and impact significant in the wave

load computation, especially near steep wave crest (Rodenbusch and Forristall 1986;
Zhang et al. 1991; Cao and Zhang 1997).

2.2.2 Hybrid Wave Model

The hybrid wave model (HWM) was developed at Texas A&M University (Zhang
et al. 1996) and proved to be accurate through the comparison with the laboratory and field
measurements (Spell et al. 1995). Unlike linear wave theory and its various empirical and
semi-empirical modifications, the continuity governing equation and free-surface boundary
conditions are satisfied up to second-order in wave steepness. This method considered the
effect of the interaction among the wave components (wave-wave interactions). The HWM
is a unified second-order theory that combines two second-order analytical perturbation
solutions (derived using the Stokes expansion perturbation approach and the phase
modulation approach) for the interaction between two free wave components. The Stokes
expansion solution is applied when the two wave frequencies are relatively close while the
solution of modulation approach is applied when the two wave components are well
separated in frequency.

2.3 Wind Force

The instantaneous wind force applied on the structure above the sea surface is
given by:

$$F_{wind} = \frac{1}{2} \rho_a A_{pw} C_{dw} \left[u_w - \frac{dx(z_{cp},t)}{dt} \right] \qquad (2.31)$$

where ρ_a is the air density, C_{dw} the drag coefficient (estimated in Chapter 5), A_{pw} the
project area of the structural element in the direction of the wind velocity (u_w), and

$\dfrac{dx(z_{CP},t)}{dt}$ the instantaneous velocity of the structure in the mean wind direction. The

instantaneous wind speed u_w is defined as the sum of the mean wind speed $\overline{U}_w$ and the

instantaneous wind velocity fluctuation about the mean u'_w.

Using an approach similar to the summation method for the random incident wave,

random wind can be decomposed into N discrete wind components:

$$u_w(z_{cp},t) = \overline{U_W}(z_{cp}) + \sum_{j=1}^{N} |u_j| \cos(w_j t + \psi_j) \tag{2.32}$$

where u_j and ω_j are the amplitude and frequency of the jth wind speed component,

respectively and ψ_j is the random phase angle. The amplitude of the wind speed of the jth

wind component (u_j) is computed following:

$$|u_j| = \sqrt{2s_w(w)\Delta w} \tag{2.33}$$

where $S_w(\omega)$ is the wind speed spectrum and $\Delta\omega$ the bandwidth.

In this study, the wind forces on the hull above the sea surface were calculated

following API recommendation (API 1996). There are several wind models for describing

the wind speed spectrum. The American Petroleum Institute (API) wind spectrum has the

following expression as seen below:

$$S_W(\omega) = \dfrac{\sigma^2(z)}{2\pi f_r [1 + \dfrac{1.5\omega}{2\pi f_r}]^{5/3}} \tag{2.34}$$

where $\sigma^2(z)$ is the variance of the wind speed at elevation (z) and f_r is a reference frequency given by:

$$f_r = \frac{0.025 U_w(z)}{z} \qquad (2.35)$$

The standard deviation of the wind speed $\sigma(z)$ is related to the wind turbulence intensity by:

$$\frac{\sigma(z)}{U_w(z)} = \begin{cases} 0.15(\dfrac{z}{z_s})^{-0.125} & for \quad z/z_s < 1 \\ 0.15(\dfrac{z}{z_s})^{-0.275} & for \quad z/z_s > 1 \end{cases} \qquad (2.36)$$

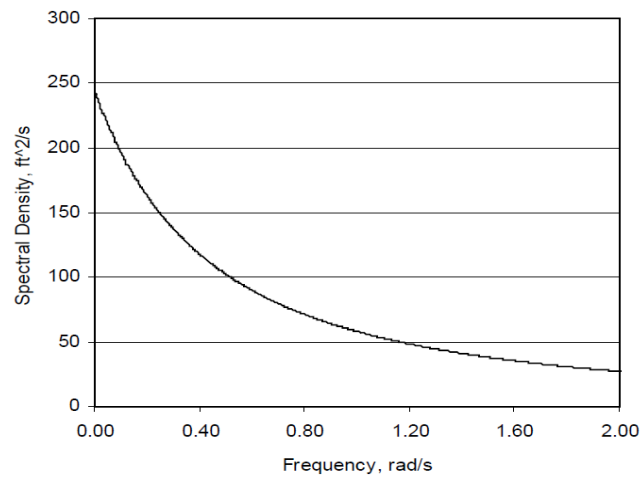where $z_s = 20$m. An API wind spectrum for $U_w = 30.48$ m/s is sketched in Fig. 2.2.

Fig. 2.2 API density spectrum of wind speed.

2.4 Current Force

The mean current force is calculated using an expression similar to the one for the mean wind force.

$$\bar{F}_{current}(z_{CP},t) = \frac{1}{2}\rho C_{dc} A_{pc}[\bar{U}(z_{CP})]^2 \tag{2.37}$$

where ρ is the water density, C_{dc} the drag coefficient (see Chapter 4), A_{pc} the projected area of the structrual element in the direction of the mean current velocity $\bar{U}(z_{CP})$.

2.5 Orcaflex

To compare the results from 'COUPLE', the author also used another similar code 'Orcaflex', a time domain program, which is widely used by the offshore industry. It is mainly used in static and dynamic analysis of a moored floating structure global motion and mooring lines.

Table 2.1 Numerical code comparison

	Orcaflex	COUPLE
Current Force	Morison equation	Morrison equation
Wave Load	Morison equation	Morrison equation
Wave Theory	Linear wave theory	Non-linear wave theory
Wave Spectrum	JONSWAP	JONSWAP
Mooring line theory	Finite difference	Finite element
Wind spectrum	API spectrum	API spectrum

The principles for the computation in 'Orcaflex' are similar to those in 'COUPLE'. However, there are still some significant differences between these two softwares. The

detailed description of the software 'Orcaflexʼ can be found in ʻOrcaflexʼ User Manual (1987-2010). The main differences together with the similarities between these two numerical codes are summarized in Table 2.1.

3   FIELD MEASUREMENT

3.1   Environment Platform Response Measurement System

The field measurements used in this study were recorded by the EPRMS and post-processed by BMT. The available records ranged from June 2007 to June 2010 were downloaded from the BMT's Client Data Center (CDC) with the permission of Anadarko Petroleum Corporation. The data used in this study including:

- Mooring Line Tensions

- Hourly Significant Wave Height and Peak Period

- The Platform Position (GPS signals)

- Platform Surge, Sway and Heave

- Roll, Yaw, Heel and Pitch

- Current Profile and direction

- Spar Platform Draft

- Wind Speed and Direction

- Hourly Spar Riser Tension

The field data not used in this study including:

- Hourly 3 Linear Accelerations and 3 Angular Velocities

- Ballast Tank Status

- Hourly Spar Platform Air Gap Height

The platform position was measured using a 6DOF accelerometer and a GPS. The current was measured at the surface by the equipment attached on the platform. The wind

was recorded by an anemometer located on the platform crane. The mooring tensions were recorded at the chain jack. For the comparison with 'COUPLE' and 'Orcaflex' the tensions recorded at the chain jack were corrected by subtracting the dry and wet weights (based on mean water level) to get the tensions at the fairlead.

3.2 Description of Post-processing

The field measurements of 'Constitution' spar were post-processed by the BMT. The errors mainly caused by the low frequency instrumentation drifts and high frequency noise components were removed. Band pass filters were also used to remove these errors. Similar detailed procedures were described in Theckumpurath (2006) and summarized below:

- The translation motions (surge, sway and heave) were obtained through the combination of two measurements: the high frequency linear translation were obtained by double integrating the accelerations in surge, sway and heave directions with respect to time and low frequency linear translations recorded by GPS signals.

- Rotation motions roll, pitch and yaw were obtained by integrating the measured angular velocities with respect to time. Before the integration, the angular velocities are filtered using a band filter in the frequency range from 0.01 Hz to 0.2 Hz.

3.3   Data Comparison with NDBC

Before the numerical simulation, the measured wind, wave and current data were compared with the related measurements obtained from National Data Buoyancy Center (NDBC) to ensure the reliability of our measurements. The author selected a nearby station (NDBC 42362) located at 27.48 North Latitude and 90.40 West Longitude. This station is located in the east of the 'Constitution', with a distance about 50 miles. Two continuous days (Feb.4 ~ Feb.5 2008) were randomly selected for the comparison.

The comparison showed that the 'Constitution' data are quite closed to the NDBC data with a difference of ±0.5 m/s for the wind speed. The difference of wind direction is about ± 20 degrees. The trend of the 'Constitution' and the NDBC wind data is very similar. The comparison was shown in the Fig. 3.1 and Fig. 3.2. Because EMPRS did not measure the wave direction, the wave direction data were obtained based on the meteorological observations in another nearby NDBC station 42002 in the southwest of the platform about 150 miles.
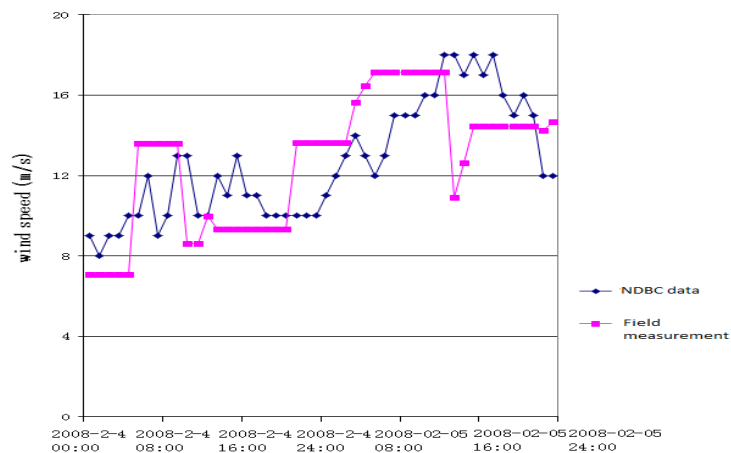

Fig. 3.1 The wind speed magnitude comparison between our data and NDBC data.
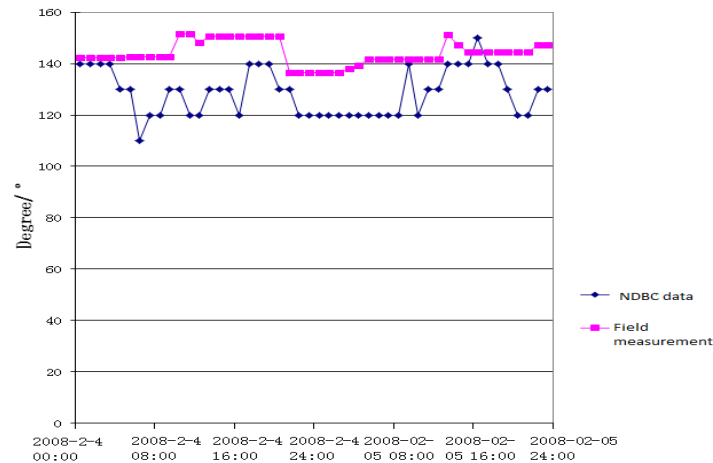
Fig. 3.2 The wind speed direction comparison between our data and the NDBC data.

3.4   Met-ocean Conditions Used for the Simulation

Two storms have been selected in the couple dynamic analysis. The first case is 'Hurricane Ike' which occurred on September 12th, 2008. The peak of Hurricane Ike passed nearby 'Constitution' on 12th of September, 2008 from 00:00am ~ 01:00am. The numerical simulation study was made particularly in this duration. The second case is a strong winter storm occurred on November 11, 2009. The peak hour of the winter storm from 12:00pm ~ 13:00pm was selected for the simulation. The direction and magnitude of the wind, wave and current are listed in Table 3.1. Because only the surface current data were provided to us, the current profile factors were given based on API design criteria (API 2INT-MET). The current profiles in the two cases were drawn in the Fig. 3.3.
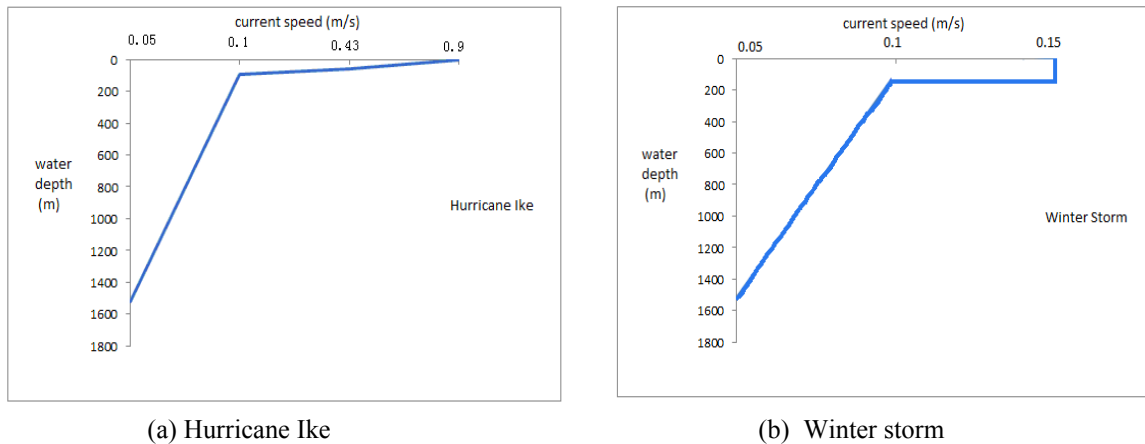
(a) Hurricane Ike   (b) Winter storm

Fig. 3.3 Current shear current profile.

Table 3.1 Environment condition

Load	Parameters	Units	Hurricane Ike	Winter Storm
Wave	Spectrum Type	-	JONSWAP	JONSWAP
	Significant Height	m	9.3	6.03
	Peak Period	sec	14.84	13.8
	Shape Factor		2.2	2.2
	Heading	deg	190	160
Wind	Spectrum Type		API	API
	Speed	m/sec	37.4	12.4
	Heading	deg	170	340
Current	Heading	deg	286	272
	Depth-Speed	m-m/sec	0-0.8	0-0.15
			61-0.43	61-0.15
			92-0.1	92-0.1
			1524-0.05	1524-0.05

3.5   Tension Data

For the purpose of corrosion protection, the tension sensors were installed at the chain jacks above the sea water level. As shown in Fig 3.4, it is clear that the tension at the fairlead should be equal to the field measurement minus the dry and wet weight of the

mooring segment between the chain jack and fairlead. More important, the measured

tension should be subtracted the coulomb friction force at the roller of the fairlead in order

to get the out board tension which is corresponding to the simulated data. Previous studies

showed that these frictions had significant impact on the measured line tensions when

comparing with the numerical results (Tahar et al. 2005; Kiecke and Zhang 2012).
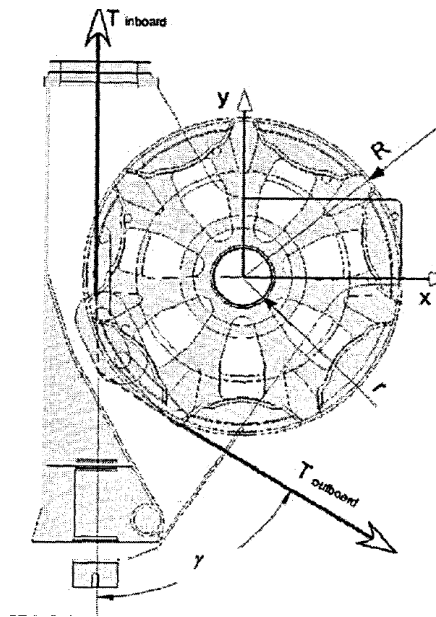
Fig. 3.4 Mooring fairlead drawing.

Although there were some previous studies on how to calculate the value of the

coulombs frictions (Tahar et al. 2005; Theckumpurath 2006), the coulomb friction

coefficient is very difficult to pinpoint because the undetermined steel corrosion and bio-

deterioration of the fairlead under the seawater environment (see Fig. 3.5). Another

difficulty in the friction coefficient calculation is that the translation motion of the platform

chain may not always exactly along the centerline of the fairlead roller that makes the friction coefficient uncertain. As a result, the friction effects were not subtracted from the field measurements for this study.

Fig. 3.5 Picture of mooring fairlead under the seawater.

4   CALCULATION PREPARATION

4.1   Estimation of Hydrodynamic Coefficient

A detailed review of the various previous studies on the related model test was conducted to predict the hydrodynamic coefficient of the spar hull and the other main sections. These studies included Magee et al. (2000), Prislin et al. (2005) and Theckumpurath (2006). For a spar platform consisted of slender column bodies, its added mass was chosen as 1. The drag coefficient and the added-mass coefficients of the mooring system have been supplied by Anadarko Petroleum Corporation.

Table 4.1 Hydrodynamic coefficients.

Spar Sections	Hydrodynamic Coefficient	
	Drag Coefficient	Added Mass Coefficient
Hard Tank	1.2	1
Truss Members	1	0.8
Soft Tank	1.2	1
Heave Plates	6	2
Mooring Chain	2.4	2
Mooring Wire	1.2	1

Also, a series decay tests were done to find out the natural periods of the platform. The free decay test in the surge, pitch and heave direction are sown in Fig. 4.1. The final values of the hydrodynamic coefficients which were used in the numerical simulation are given in Table 4.1.
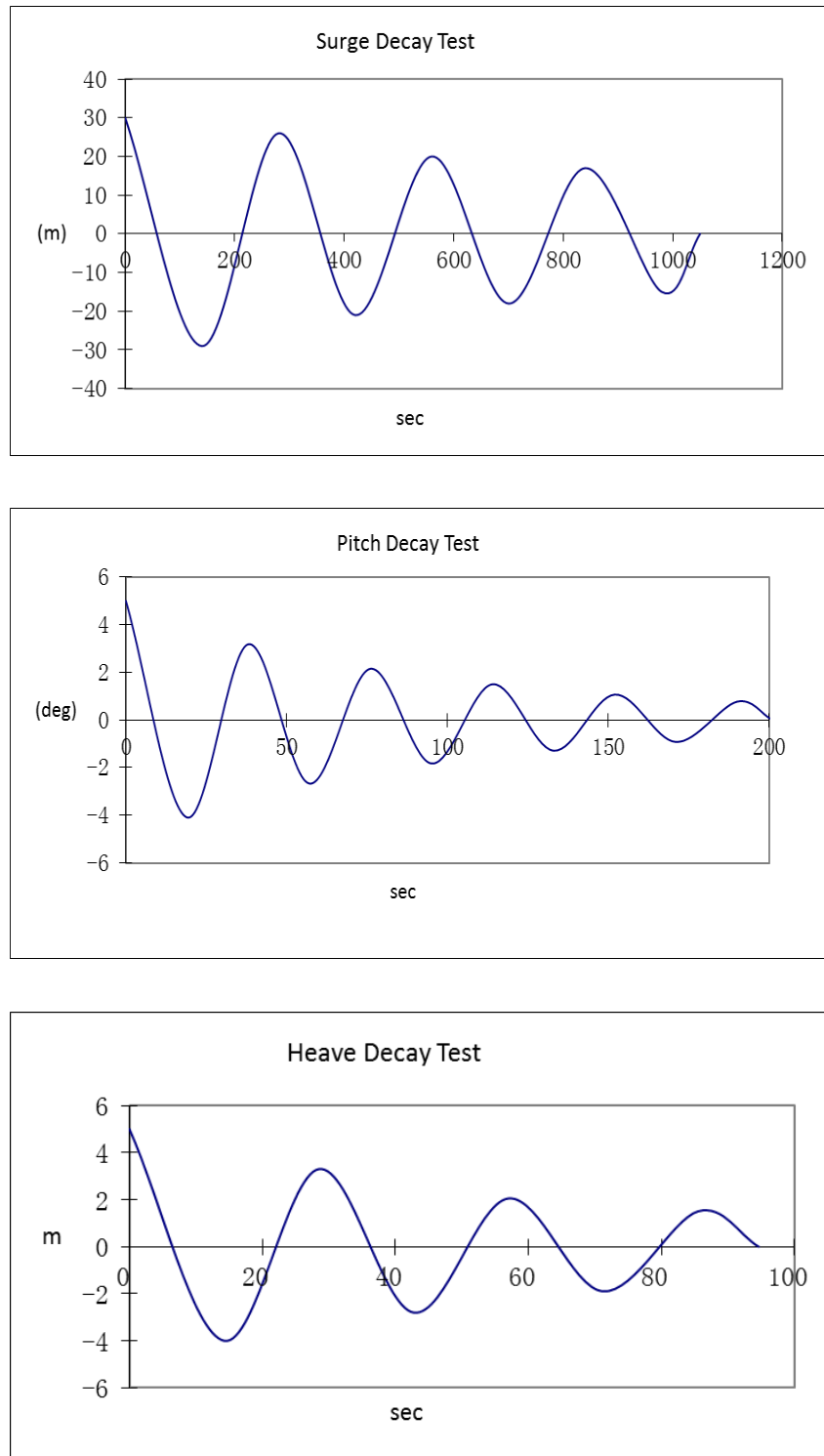
Fig. 4.1 Results of free decay test.

4.2   Equilibrium Position

4.2.1   Equilibrium Position before Storms

During the operation, the mooring line payouts may be changed instead of remaining the same in order to adapt the operation requirement and environment condition (wind, wave and current). As a result, the platform 'equilibrium' position (when no external force except mooring/SCR forces is applied on the structure) was not exactly at the GPS initial point (0, 0) and may be changed during the whole period. Unfortunately, the mooring payouts changes were not always recorded in field data although they were supposed to be recorded. To find the 'equilibrium' position and mooring line payouts before hurricane 'Ike' and the selected winter storm, the author conducted a series of simulation and examination.

First, the author selects a one hour period (13:00 – 14:00 pm on the 6th of September 2008) about 6 days before the hurricane Ike and another period near the (8:00 – 9:00am on the 26th of August 2009) about 15 days before the winter storm. During these particular selected periods, the magnitude of the wind, wave and current were very weak as shown in Table 4.2.

Secondly, by scrutinizing the field measurement data in these periods, it was found that the global motions of the spar platform in these two periods were indeed very small due to the weak environment impact. Also, because the time lapses between the time we examined the 'equilibrium' position and the time when we conducted the couple dynamic analysis of the spar during the storms were very short (6 and 15 days), the mooring line payouts can be considered to remain unchanged. As a result, these platform positions can

be considered as at the 'equilibrium' positions before Hurricane 'Ike' and winter storm for the computation of the spar coupled dynamic performance during the peak hour of hurricane 'Ike' and the selected winter storm.

Table 4.2 Environment condition for 'equilibrium' position

Mean values		Before Winter Storm	Before IKE
Wind Speed	(m/s)	0.2	0.2
Current Speed	(m/s)	0.05	0.04
Wave H_s	(m)	0.1	0.22

4.2.2 Mooring Line Payout Adjustment

The author adjusted the length of the platform chain from the initial payouts to satisfy the equilibrium positions and the tension measurements. This is possible when the mooring platform chain were changed through the roller in the fairlead during the operation. The mooring platform chain payouts given by the design and the estimated payouts before Hurricane 'Ike' and winter storm (WS) are given in Table 4.3.

Table 4.3 Estimate mooring line payouts before Hurricane Ike and WS.

Mooring line #	Design (m)	Ike (m)	WS (m)
1	137.2	121.6	118.9
2	137.2	118.3	125.0
3	137.2	117.3	115.8
4	91.4	70.1	70.1
5	91.4	70.1	70.1
6	91.4	70.1	61.0
7	91.4	85.3	82.3
8	91.4	85.3	88.4
9	91.4	82.3	85.3

To verify the mooring line payouts in the two 'equilibrium' positions respectively right before hurricane Ike and WS, the author calculated the mooring line tensions (at the fairlead) in these positions with the numerical software 'COUPLE' (by inputting the 'equilibrium' positions and the estimated mooring payouts) and compared with the mean tension of each mooring line recorded in the field measurement. The mooring line configurations were based on the design document provided by APC (see Chapter 1). Each of the mooring line had associated depth and line lengths for the mid-section and anchor chain segment above the seabed. However, as mentioned before, only the length of the platform chain at the platform fairlead was modified by the author. In addition, it is necessary to point out that the wet and dry chain weights were already subtracted from the measured tension at the chain-jack in order to get a comparison with the simulated tension which was corresponding to the tensions at the fairlead. The mooring line and the corresponding numerical model used in 'COUPLE' are shown in Fig. 4.2. The measured and simulated mean tensions were compared resulted in Table 4.4.
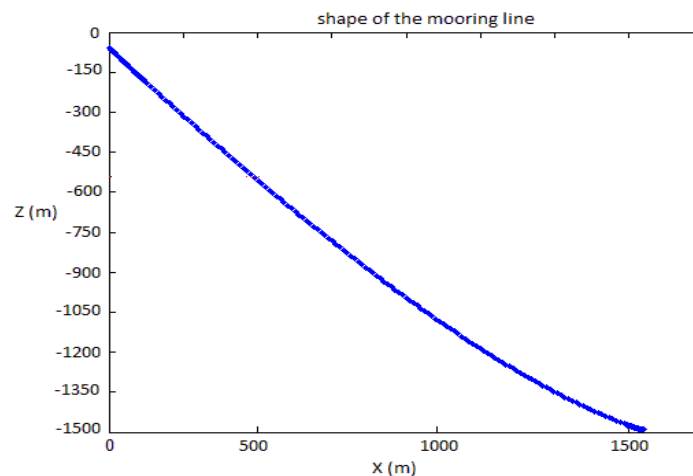

Fig. 4.2 Numerical mooring line configuration.

Table 4.4 Mooring line tension resultant.

Before Hurricane Ike (kN)									
Line #	1	2	3	4	5	6	7	8	9
Measured	2917	2709	3031	2637	2665	2807	2817	2716	2710
Simulated	2812	2859	2856	2499	2474	2680	2961	2822	2810
Diff	-105	150	-175	-138	-191	-127	144	106	100
Error	-3.6%	5.5%	-5.8%	-5.2%	-7.2%	-4.5%	5.1%	3.9%	3.7%
Before Winter Storm (kN)									
Line #	1	2	3	4	5	6	7	8	9
Measured	3043	2733	2979	2548	2593	2769	2802	2633	2705
Simulated	2962	2705	2966	2443	2449	2759	3007	2754	2810
Diff	-81	-28	-13	-105	-144	-10	205	120	105
Error	-2.6%	-1.0%	-0.5%	-4.1%	-5.5%	-0.4%	7.3%	4.6%	3.9%

The comparisons shown in Table 4.5 indicated that the simulated tension of each mooring line is in satisfaction agreement with the corresponding measurement in the selected 'equilibrium' spar position. The maximum difference between the numerical results and the field data measurement is no more than 7.3%. As a result, the mooring line payouts in the 'equilibrium' position of the numerical model can be considered valid and will be used in the dynamic analysis for the comparison of the 6DOF motion analysis in Chapter 6. Also by distributing all the simulation mooring/SCR tensions in the equilibrium positions before hurricane 'Ike' and winter storm into x-axis and y-axis, it was found that the resultant of the mooring/SCR forces in x- and y-axis are very small and nearly equal to zero (see Table 4.5).

Table 4.5 Mooring line tension comparison.

	Hurricane Ike			Winter Storm		
	Tension (kN)	Force_x (kN)	Force_y (kN)	Tension (kN)	Force_x (kN)	Force_y (kN)
mooring line 1	2812	1408	-76	2962	1529	-87
mooring line 2	2859	1438	-199	2705	1306	-184
mooring line 3	2856	1415	-321	2966	1499	-344
mooring line 4	2499	-573	-1119	2443	-555	-1076
mooring line 5	2474	-656	-1047	2449	-648	-1029
mooring line 6	2680	-828	-1103	2759	-887	-1175
mooring line 7	2961	-911	1316	3007	-927	1351
mooring line 8	2822	-743	1289	2754	-710	1244
mooring line 9	2810	-621	1326	2810	-629	1355
SCR 1	378	24	-62	378	22	-63
SCR 2	129	11	-21	130	10	-21
Sum		-37	-17		11	-28

4.2.3 Verification of Equilibrium Positions

To verify the equilibrium position, the author also selected another two cases (18:00 ~ 19:00 pm on the 6th of September 2008 and 8:00 ~ 9:00 am on the 24th of August 2009). In these two additional selected cases, the magnitude of wind, wave and current were also very small but relatively stronger than the ones in the previous related 'equilibrium' cases. These environment conditions are coined as the 'near-equilibrium' condition. The corresponding positions of the spar platform in these two cases comparing with the 'equilibrium' positions were depicted in Fig. 4.3. The magnitude of wind, wave and current of the 'equilibrium' condition and 'near-equilibrium' condition are compared in Fig. 4.4.
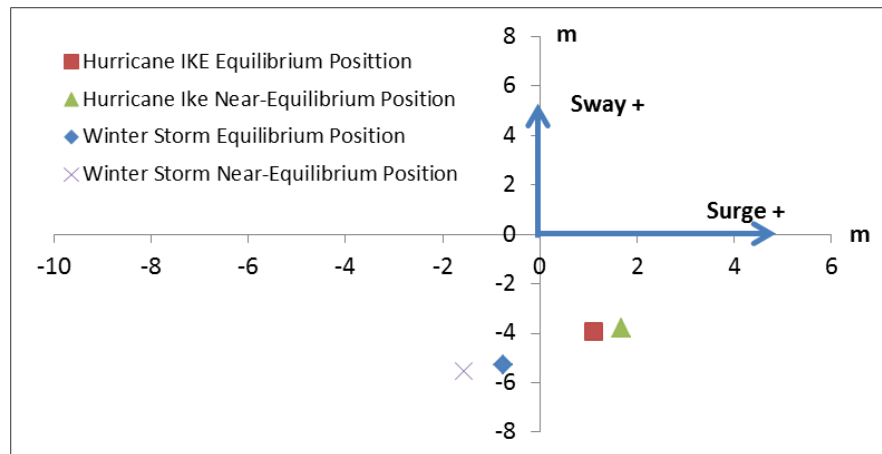
Fig. 4.3 Spar 'equilibrium' and 'near-equilibrium' positions.

The above figure shows that the equilibrium positions and near-equilibrium ones in the corresponding cases are very close but not exactly at the same location. These differences are mainly because of the environment impact. To verify this, the author conducted the following verification and examination.

(a) Before Ike

(b) Before winter storm

Fig. 4.4 Near-equilibrium and equilibrium environment before winter storm.

First, to get the resultant force from mooring line and SCRs, the author drives the spar platform from the 'equilibrium' position to the related 'near-equilibrium' position by applying a steady force on the platform in numerical codes. As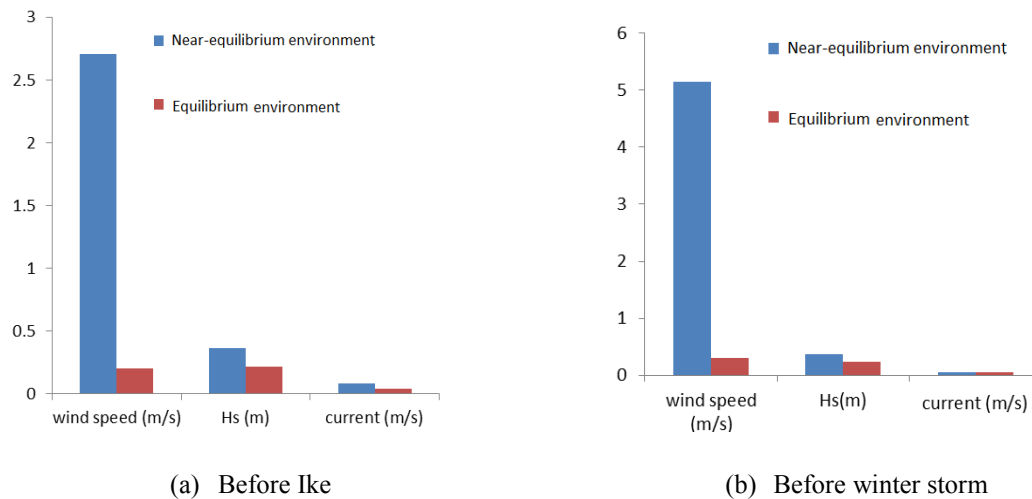 a result, the resultant mean tension from mooring line and SCRs in this period should be equal to the applied force with an opposite direction.

Then by using the Morison equation, wind effective coefficient (obtained in Chapter 5) and wind/current mean speed in 'near-equilibrium' position, the author calculated the mean current force and the mean wind force applied on the platform. The mean wave drift force can be neglect in these conditions since the significant wave height in both cases are very small ($H_s = 0.2$m). The comparison between the environment forces and mooring line forces are listed in Table 4.6.

Table 4.6 Mooring tensions & environment force.

	Before Hurricane Ike	
	Force in Surge Direction (kN)	Force in Sway Direction (kN)
Environment Force	67.3	7.9
Mooring Force	-74.8	-7.3
Difference	10%	9%
	Before Winter Storm	
	Force in Surge Direction (kN)	Force in Sway Direction (kN)
Environment Force	-87.3	-5.3
Mooring Force	76.8	4.9
Difference	12%	6 %

From the tables above, we can concluded that the mooring/riser tension and evironment forces compared very well in both x- and y-axis with a maximum difference no more than 12%. Also, the directions of the mooring/riser force and the environment loads

in the two 'near-equilibrium' positions are virtually opposite as shown in Fig. 4.5. As a result, it is verified that the 'equilibrium' postion of the spar platform can be considered as valid and used in the follwing numerical simulation of the spar platform.
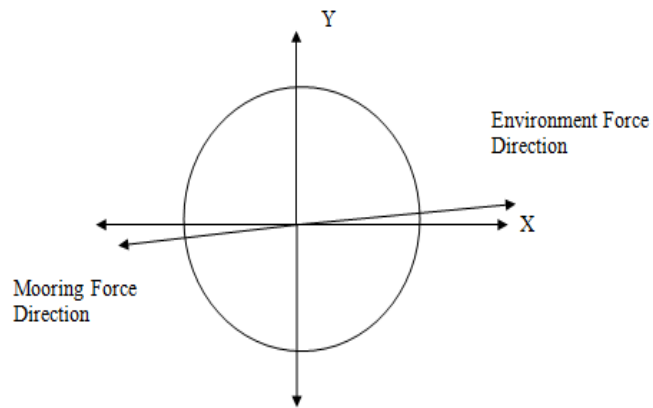
(a) Hurricane Ike
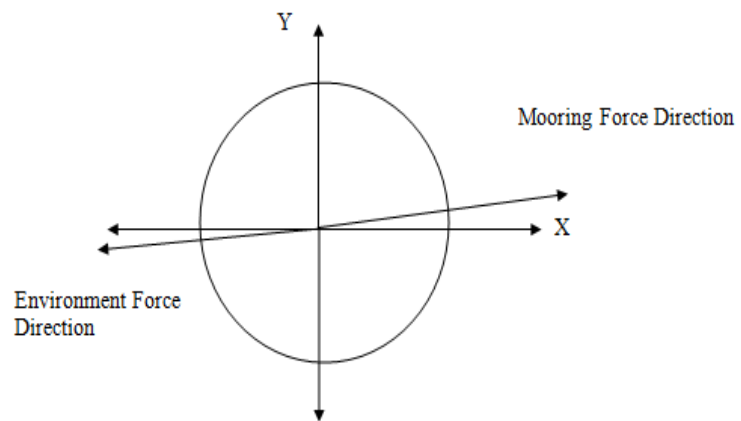
(b) Winter storm

Fig. 4.5 Force directions before Ike and WS

5   WIND IMPACT AREA AND WIND COEFFICIENT

The wind speed and direction were recorded using an anemometer on the platform crane. The wind direction with respect to the global coordinate was derived based on anemometer heading, platform heading and a crane encoder (a pinion gear that measures the rotation of the crane from a specific point).

5.1   Wind Effective Area

5.1.1   Definition of Environment Coordinates

The measured wind direction is defined in a different way from that of measured wave or current (see Fig. 5.1). For the consistency of computing the environment loads on the spar platform, the measured wind direction coordinate is redefined in the same way as the wave and current.

As shown in Fig. 5.1, the environment global coordinates are defined such that X-axis is positive towards the east and Y-axis is positive towards the north. Z-axis is positive up and the origin is located at the calm water level. Directions for waves, current and wind are defined as the direction in which they are advancing.

5.1.2   Wind Pressure Center and Impact Area

Based on the simplified drawings of the topside configuration as shown in Fig. 5.2 and Fig. 5.3, the author estimated the geometry center of the topside in the north and east side. The detail descriptions of the wind area in the topside and wind pressure center are described in Appendix A.

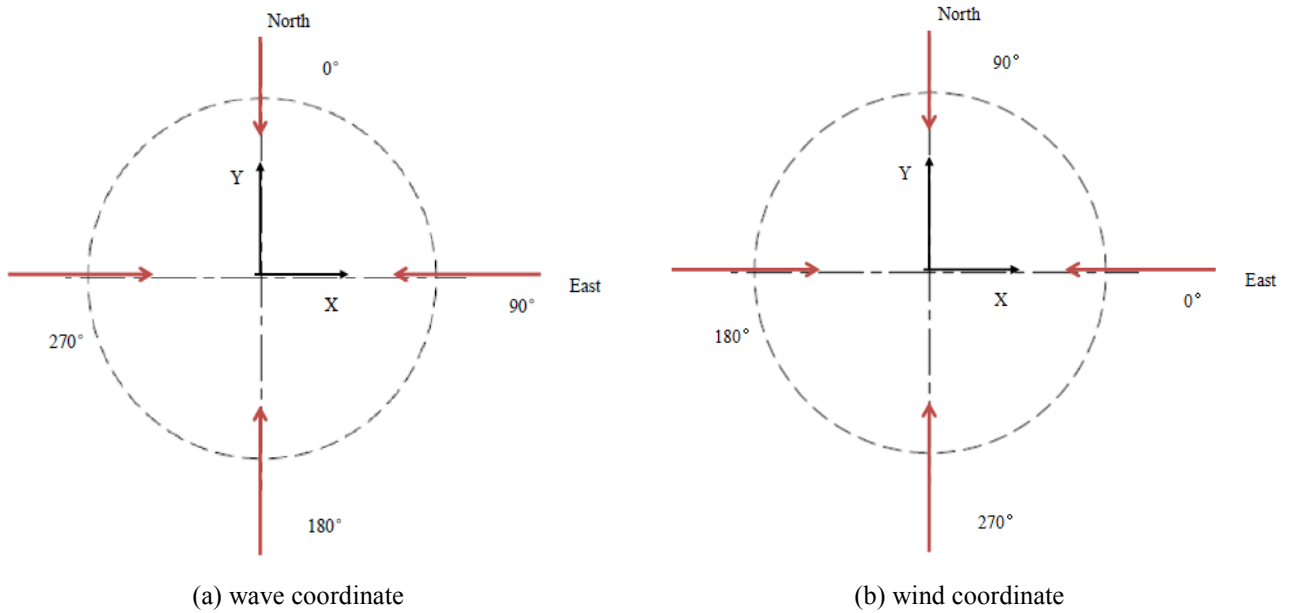(a) wave coordinate   (b) wind coordinate

Fig. 5.1 Definition of the wave and wind coordinates.
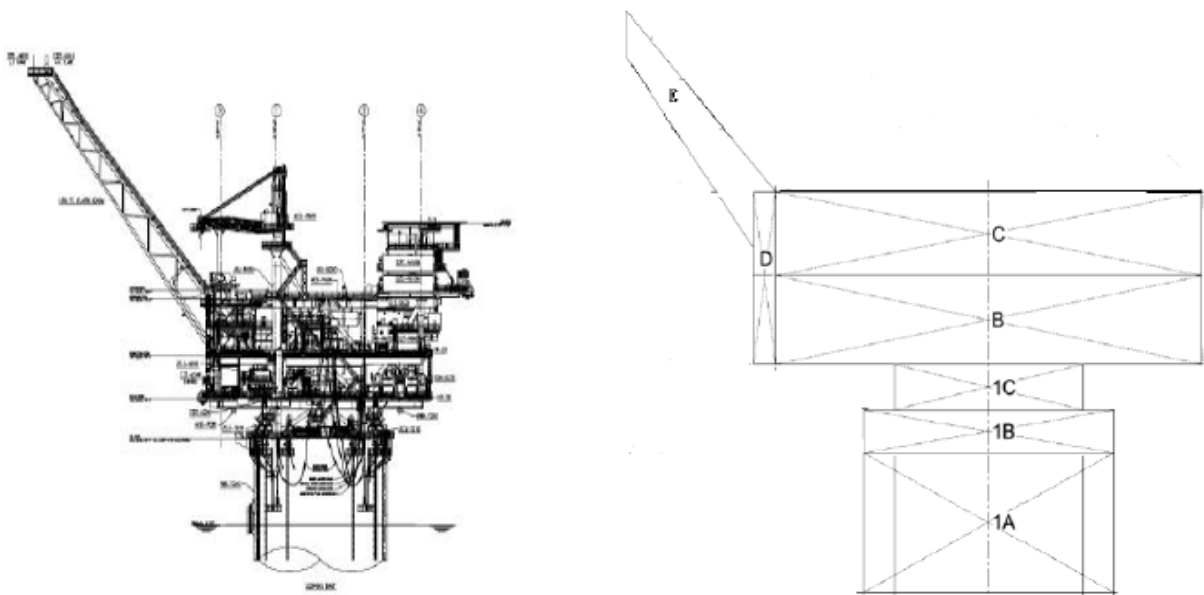
Fig. 5.2 The configuration and simplified configuration of the spar east side.
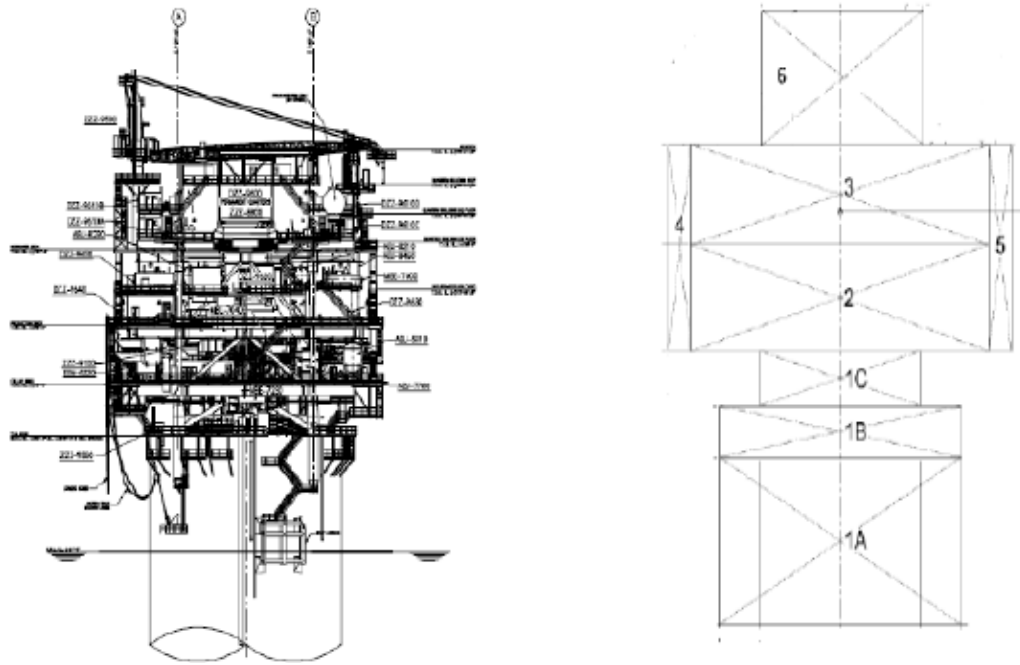
Fig. 5.3 The configuration and simplified configuration of the spar north side.

From the calculation described in Appendix A, the total wind impact areas were obtained. The geometric centers of each side were also calculated which are (0, 0, 30.7 m) in the north side and (0, 0, 31.9 m) in the east. However, because the un-uniform wind speed is assumed in the computation of wind loads on the topside, the actual center of wind pressure should be slightly higher than the geometric center and were then defined as (0, 0, 31.9 m) in both sides. These results have very significant effect on the spar roll and pitch motions and will be used in both 'COUPLE' and 'Orcaflex' to simulate the wind loads on the spar platform.

5.2   Wind Load Coefficient

5.2.1   Wind Drag Coefficient

The wind drag coefficient denoted by C_d is a dimensionless parameter which is defined in equation 5.1.

$$C_d = \frac{2F_{wind}}{\rho u^2 A}$$

(5.1)

where:

F_{wind} is the total wind force applied on the structure

ρ is the density of the air

U is the wind speed relative to the spar platform at the wind pressure center

A is the projection area of the Spar topside and hull normal to the wind direction

$$C_e = \frac{1}{2}\rho A C_d$$

(5.2)

where C_e is known as the effective wind load coefficient which is a dimensional parameter including the effect of wind impact area.

In general, a wind tunnel model test is conducted for the computation of the effective wind load coefficient. In this study, because the wind tunnel test data are not available to us, the author estimated the effective wind load coefficient for the spar platform based on the field measurement. These results will then be used in the spar global motion and mooring tension analysis. The procedure of the estimation is described below.

5.2.2   Estimation of Wind Effective Load Coefficients

To estimate the effective wind load coefficients, the author chose an hour when wind was relatively strong while the magnitude of the wave and current were relatively weak. First, the author selected one hour duration (15:00 pm ~ 16:00pm on 7th of September 2008) when the environment forces from wave and current are very weak relatively to the wind force (V_{wind} = 5.25 m/s, $V_{current}$ = 0.03m/s, H_s = 0.1m). Based on the calculation of tensions in each mooring line (obtained from 'COUPLE' by inputting the mooring configuration, the position of the spar platform and a steady force which represents the environment loads), the author calculated the direction and magnitude of the mean tensions from each mooring line and SCR forces together with the *x*-axis and *y*-axis tension components (see Table 5.1). The wind direction from the field measurement and the resultant of the total mooring/SCR force are shown in Fig. 5.4

Table 5.1 Mooring/SCR tensions.

Mooring Line #	F_{total} (kN)	$F_{vertical}$ (kN)	$F_{horizontal}$ (kN)	F_{surge} (kN)	F_{sway} (kN)
Line01	2798	2415	1398	1396	-75
Line02	2843	2444	1439	1426	-197
Line03	2841	2442	1439	1403	-318
Line04	2504	2168	1261	-575	-1122
Line05	2479	2153	1240	-658	-1051
Line06	2603	2237	1342	-806	-1073
Line07	2972	2502	1609	-917	1322
Line08	2830	2405	1494	-748	1294
Line09	2775	2368	1447	-616	1310
SCR 1	378	372	67	22	-63
SCR 2	130	127	23	10	-21
Total				-63	7
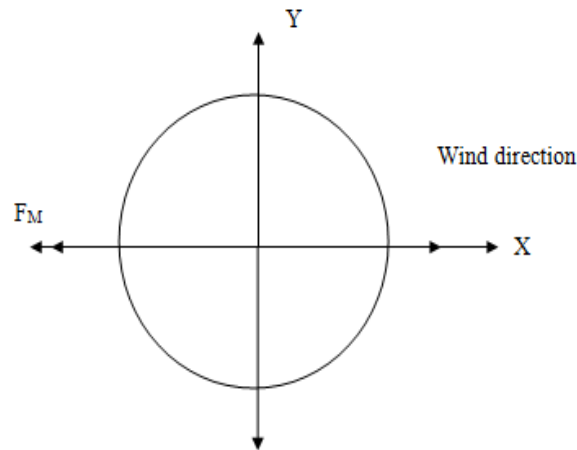
Fig. 5.4 Directions of the wind and mooring force.

It is clearly shown that the wind direction and the direction of the restoring forces provide by mooring lines and SCRs are almost opposite. After distributing the mooring force on the x- and y-axis, the effective wind coefficient C_{ex} and C_{ey} of the platform can be estimate by using the wind coefficient equation 5.2. The final result of the effective wind coefficient in the x-axis and y-axis (C_{ex} and C_{ey}) are shown in Table 5.2.

Table 5.2 Wind coefficient in wind direction 0 degree.

Source	F_x (kN)	F_y (kN)
Mooring riser Forces	-63	7
Current Force	0.08	-7
Wind Force	62.92	0
Effective Wind Coefficient	2.27	0

Repeating the procedure for four more different cases which have the similar environment condition but the wind directions are different, the wind load coefficients as a function of the wind direction θ were calculated and presented in Table 5.3. Because of the

approximate symmetry of the topside with respect to the *x*-axis, only the values for the wind direction from 0° and 180° were calculated. After interpolating the result, the final wind coefficients are plotted in Fig. 5.5.

Table 5.3 Effective wind coefficient

Wind Direction (θ)	$C_{ex}(\theta)$	$C_{ey}(\theta)$
Degree	kN/(m/s)^2	kN/(m/s)^2
0	2.27	0
30	1.78	1.18
60	0.87	2.07
90	0	2.17
120	-0.87	2.07
150	-1.60	1.25
180	-2.27	0

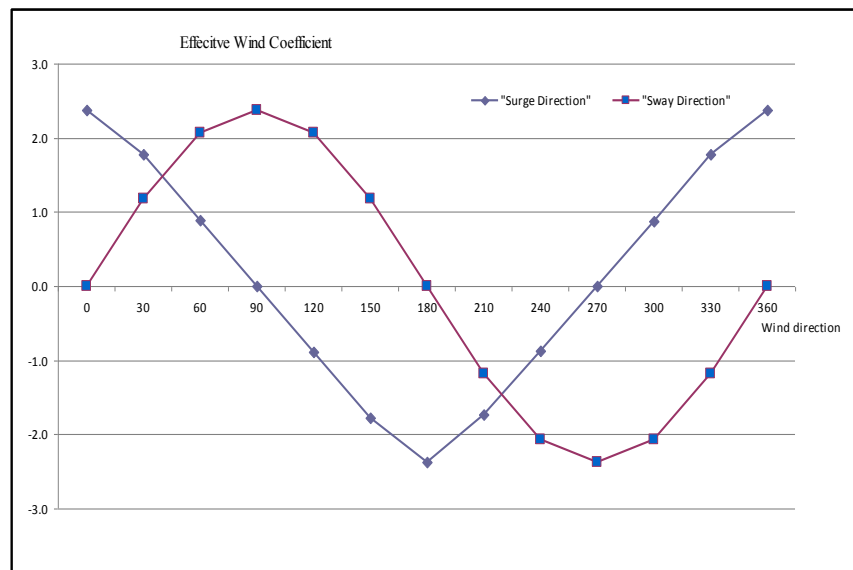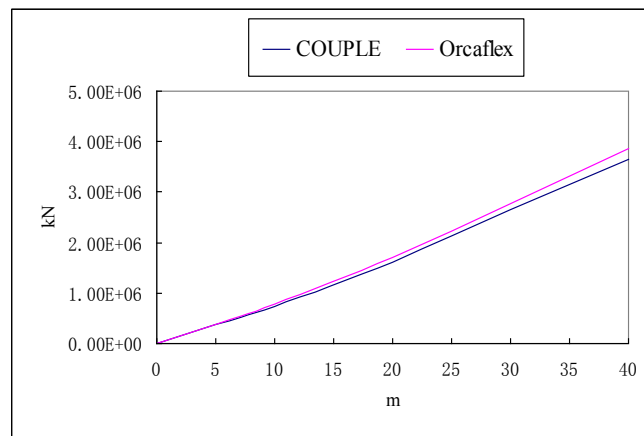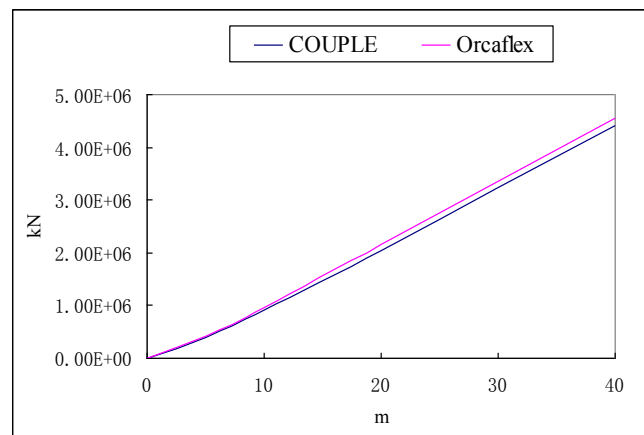Fig. 5.5 Effective wind coefficient for 'Constitution'

6   RESULT AND COMPARISON

6.1   Mooring Line Stiffness Comparison

The mooring stiffness curve of the spar was computed using both 'COUPLE' and 'Orcaflex'. The stiffness curves from two numerical codes were plotted versus the spar displacement in Fig. 6.1.

(a) Surge

(b) Sway

Fig. 6.1 Mooring stiffness in surge & sway directions.

From comparison, it is clear that the numerical results obtained using the two codes are in a good agreement. The sway direction mooring line stiffness is slightly higher than that in the surge direction. That could be explained by the mooring line arrangement which is shown in section 1.2.2. The restoring forces of mooring line 7, 8 and 9 and the steel catenary risers are mainly contribute to the sway direction while those of the other mooring lines contribute to both surge and sway directions.

In addition, from the comparison, the predicted mooring stiffness difference using 'COUPLE' and 'Orcaflex' was within 5%. The main reason for this difference probably comes mainly from the different mathematic simulation methods of mooring line and SCR system. This result could also explain the differences in the dynamic analysis of the mooring line tensions, which will be shown in section 6.3.4 and 6.4.4.

6.2   Introduction Couple Dynamic Analysis

The results of the coupled dynamic analysis of the spar hull interacting with its mooring/riser system using 'COUPLE' and 'Orcaflex' were present in Section 6.3 during the peak hour of hurricane 'Ike' and Section 6.4 during the peak hour of the selected winter storm. The simulated results included the 6DOF global motions of the platform and mooring tensions at the fairlead. These numerical results from 'COUPLE' and 'Orcaflex' were then compared with the corresponding field data measurements. Because Top Tension Riser (TTR) configuration data were not available to us, TTR system was approximated as a steady force in heave direction, which was obtained from the field measurement. The coupling effect of the TTR system with the platform was not considered in this study.

6.3   Hurricane Ike

6.3.1   Translation Motions Comparison

In general, the global motions of a rigid structure have six degrees of freedoms, that is, surge, sway, heave, roll, pitch and yaw. In this section, the simulation results of these motions were obtained from the numerical codes, 'COUPLE' and 'Orcaflex'. In the case of 'Orcaflex', two different modifications of LWT were used to compute the wave kinematics used in the Morison equation (wheeler stretching (WL) and linear extrapolation (LE)). Various statistics of the global motions were obtained including the maximum, minimum, mean, standard deviations.

From Fig. 6.2, it is clear that the simulated translation motions (surge sway and heave) predicted by both codes compares well with the field measurement. The mean values and standard deviations of all translation motions matched very well with the field measurement data. The maximum magnitude of the simulated motions in negative surge direction in 'COUPLE' is 7.6% higher than the corresponding field measurement while the other two modifications of LWT in 'Orcaflex' is 5.5% (WL) and 6.2% (LE), respectively, higher than the field measurement. In sway direction, the maximum magnitude of the numerical result from 'COUPLE' is 4% lower than the field measurement while two modifications of LWT in 'Orcaflex' are 7% (LE) and 8% (WL) lower than the corresponding field measurement. These discrepancies are expected as the magnitudes and directions of wind, wave and current might not remain the same and vary irregularly during the peak hour of the hurricane. However, in the numerical simulations, the wind, wave and current directions were approximated as unidirectional and the magnitudes of the

(a) surge

(b) sway
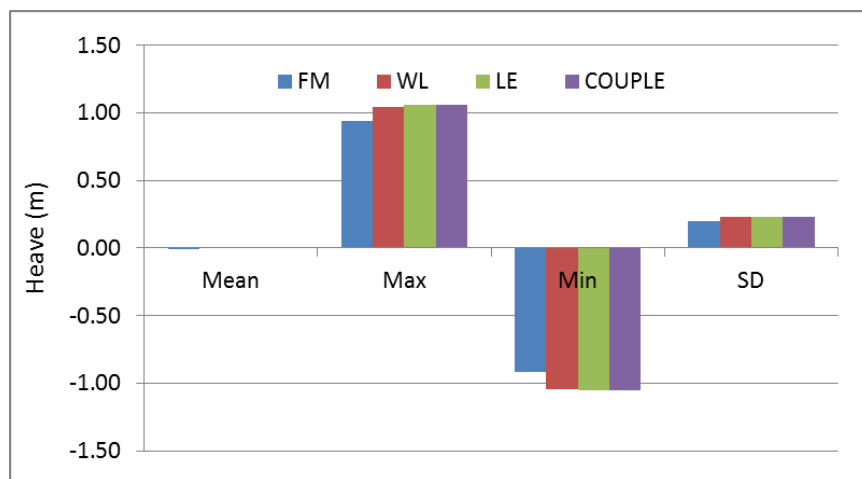
(c) heave

Fig. 6.2 Statistic comparison of translational motions during Hurricane 'Ike'.

environment followed the empirical spectrum (JONSWAP) and API wind spectrum (see Chapter 3). Also, the current were treated as steady current which neglects the fluctuation in the current.

On the other hand, the magnitudes of maximum results in the heave direction from both numerical codes were larger than the field measurement data with a difference about 15% in 'COUPLE' and 14.2% for 'Oracflex' (both WL and LE). These differences are mainly because the uncertainty of the ocean environment condition and the coupling effect between TTR and the spar platform was not considered.

6.3.2   Rotation Motion Comparison

The coupled dynamic analysis results of the spar platform rotational motions (roll, pitch and yaw) and the corresponding field data were compared in the following Fig. 6.3.

As shown in the Fig. 6.3, it is clear that the simulated results in roll and yaw directions compared reasonable well with the field data while the predictions in pitch direction are much larger than the field data. The simulated results in roll direction are larger than the field data about 11% in 'COUPLE', 13% in 'Orcaflex' (LE) and 11% in Orcaflex (WL) in magnitude. The magnitudes of the simulated pitches from both numerical codes, which were the dominant rotation in the case of hurricane 'Ike', are nearly 30% larger than the field measurement. These differences are mainly resulted from the coupling effects of TTR, which were not simulated in the numerical models. This could also explain the larger standard deviation of pitch than the field measurement while the other motions showed a reasonable agreement with the field measurement in standard deviations. Also, the yaw displacements in both numerical models are larger than the field
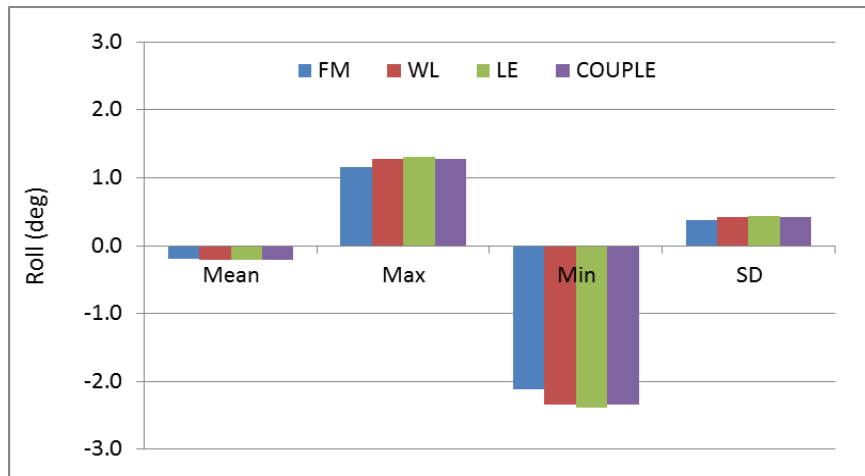
(a) Roll
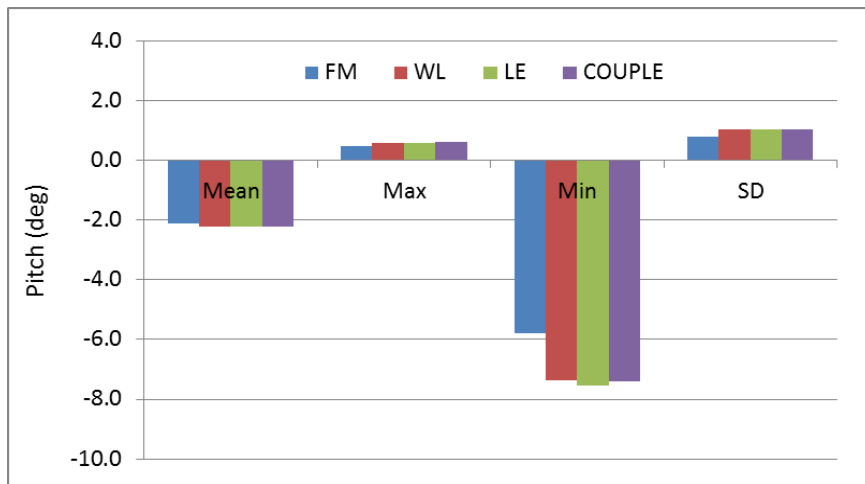
(b) Pitch

(c) Yaw

Fig. 6.3 Statistic comparison of rotational motions during Hurricane 'Ike'.

measurement with a difference of 14%. These differences are mainly due to the coupled effect from the pitch and roll modes and the friction of the TTR buoyancy can that was not considered in this model.

6.3.3 Power Spectrum Comparison

The surge spectrum in Fig. 6.4 clearly showed that the simulated results matched very well with the filed measurement in both low frequency ($\omega = 0 \sim 0.1$ rad/s) and the wave frequency range ($\omega = 0.4 \sim 0.6$ rad/s). In addition, the coupling effect from the spar pitch is also matched well near the natural frequency of the spar pitch ($\omega = 0.1 \sim 0.2$ rad/s). In addition, because of the wind, current and wave directions during the one-hour period varied randomly which is extremely difficult to simulate, there existed some discrepancy in both the low-frequency motions and the high-frequency motions.

In addition, the surge motion results from 'Orcaflex' (both WL and LE) were smaller than the ones from 'COUPLE' and the field measurement in the low frequency range. It is known that the large amplitude drift motion for the spar platform near the resonant frequency comes mainly from the wind loading, current loading and nonlinear wave loading due to the wave-wave and wave-body interactions (Newman 1974; Pinkster 1980). Since the simulation of the wind and current and computation of their loads used in both numerical codes are the same, the differences can be understood as mainly from the nonlinear wave force. It is known that modified linear wave theories could not consider the second-order temporal acceleration force which is the major contributor to the second-order different frequency force (Cao and Zhang 1997) which could be the main reason for this discrepancy.
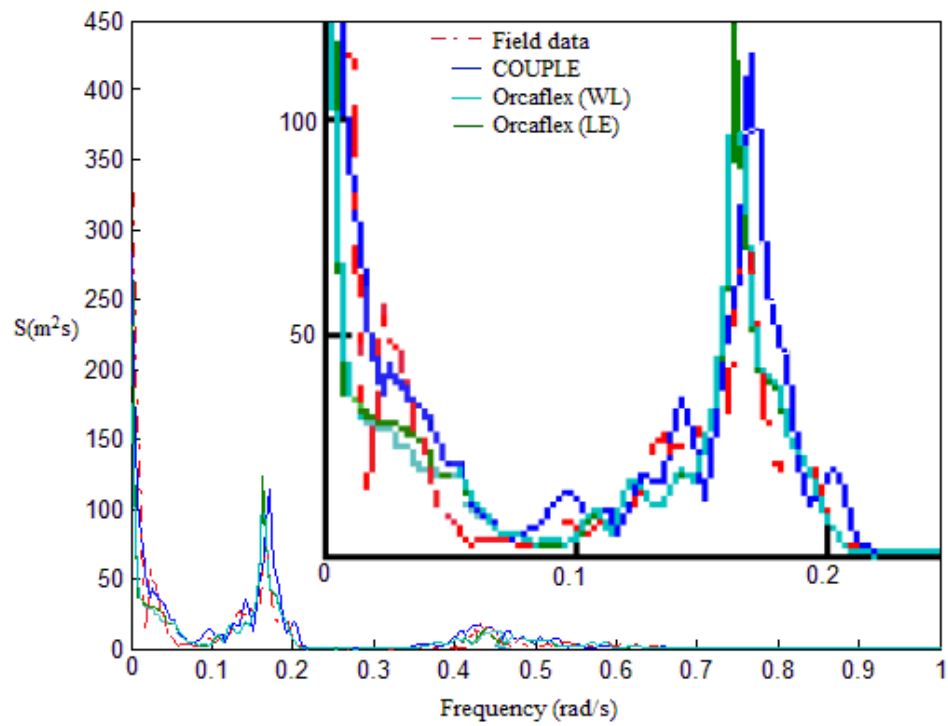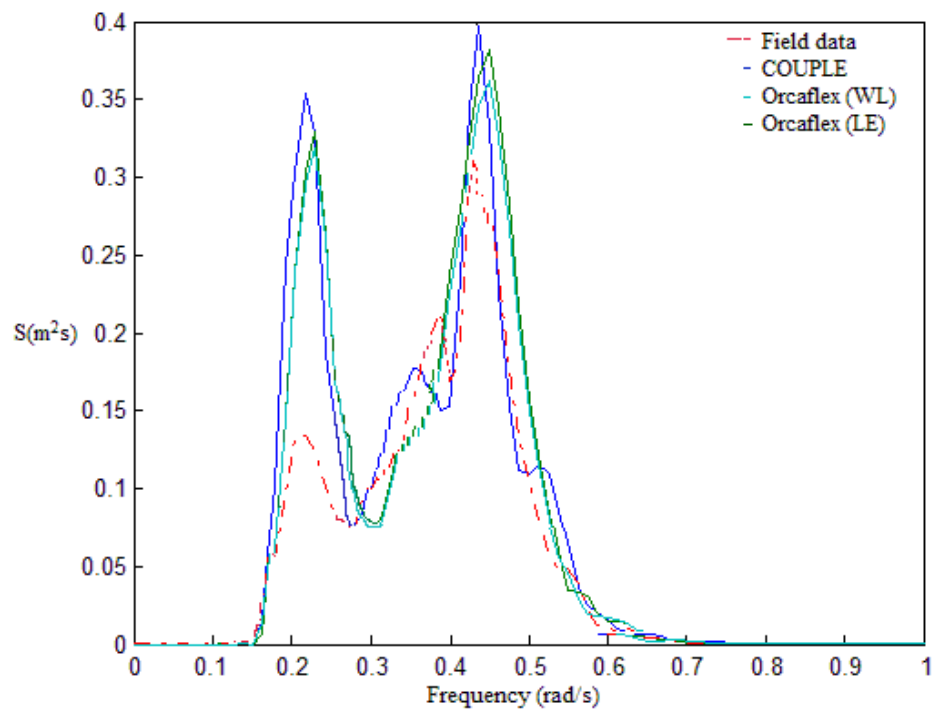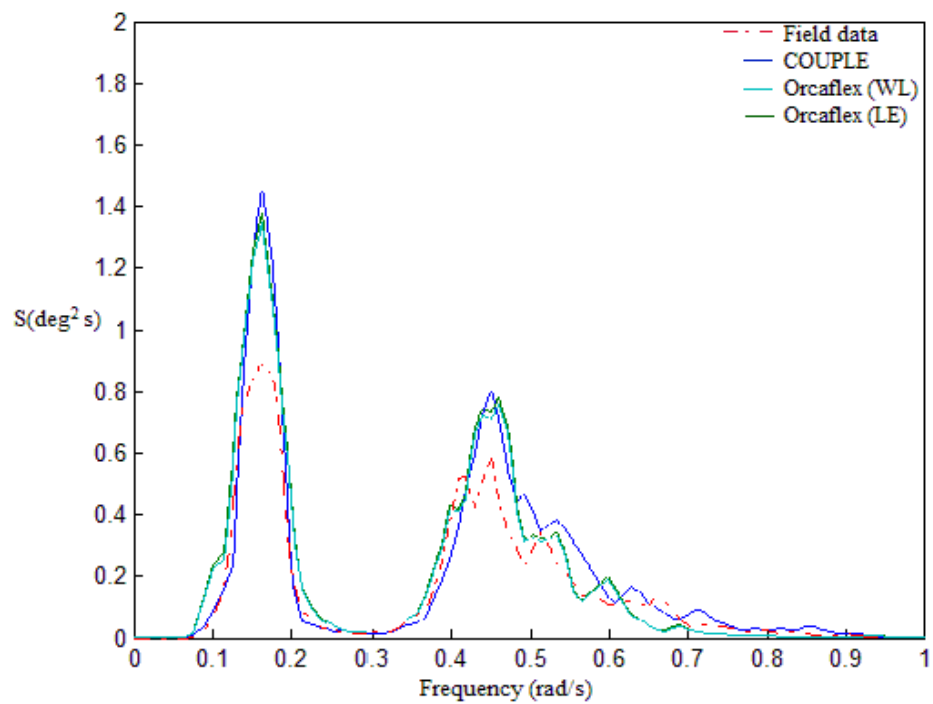
(a) Surge
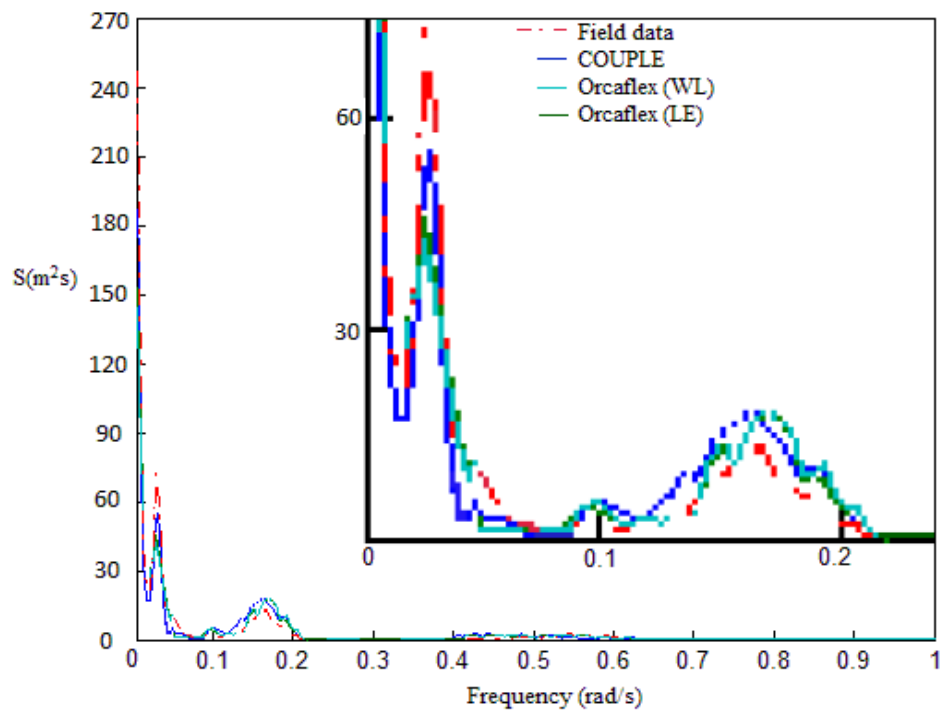
(b) Sway

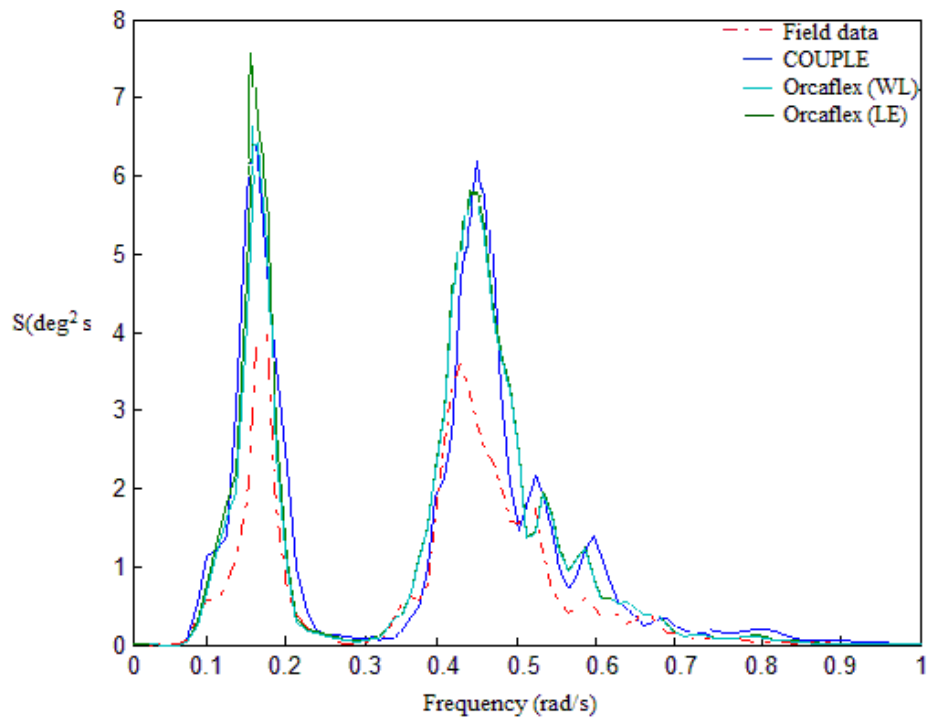Fig. 6.4 Comparison of 6DOFs spectra during Hurricane 'Ike'.
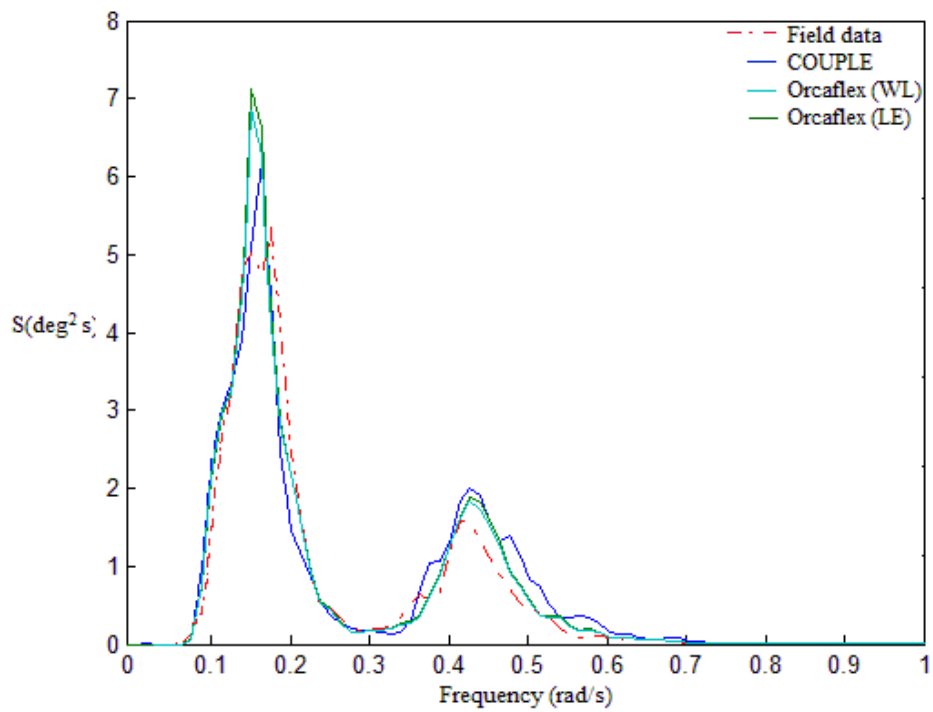
(c) Heave

(d) Roll

Fig. 6.4 Continued.

(e) Pitch

(f) Yaw

Fig. 6.4 Continued.

For the sway motion, it is found out that the numerical results in sway direction matched very well with the field measurement in the low-frequency, pitch/roll coupling effect frequency and the wave frequency. Since the wave direction (190 deg) was mainly along the surge direction, the energy magnitude at the wave frequency (0.4 ~ 0.6 rad/s) in the sway spectra was much smaller than the corresponding one in surge spectra. As expected, the discrepancy between 'COUPLE' and 'Orcaflex' in the low frequency range which mainly comes from the nonlinear wave forces became smaller comparing with the one in surge direction.

The comparison in the heave, roll and pitch spectra showed that the numerical results near the resonant frequency of the heave, roll and pitch motions, as well as the wave frequency overestimated the corresponding motions in the field data (especially in the pitch which is the main rotation of the spar in the case of hurricane 'Ike'). These differences mainly come from the missing consideration of the coupling effects of the TTR system in the numerical model. The differences between the results of the two numerical codes near the natural frequency of pitch and roll are mainly due to the fact that modification of LWT could not accurately predict the nonlinear drift motions of the platform in roll and pitch (Cao and Zhang 1997). Besides, the yaw motions from both numerical models matched reasonably well with the field data in both its natural frequency range and wave frequency range. The slight difference between the numerical results and field data are mainly due to the coupling effect of the pitch and roll motions.

From the spectra comparisons, we can conclude that the numerical results from nonlinear wave model (HWM) in 'COUPLE' and the results from modified linear wave

models used in 'Orcaflex' both match reasonably well with the field measurement in the wave frequency range. However, 'Orcaflex' using the modification of LWT underestimated the slow-drift motion of the platform in the low frequency range while the 'COUPLE' using nonlinear HWM matched better with the field measurement. Due to the missing consideration of the interaction of TTR, the spar heave, roll and pitch motions were all higher than the corresponding field data.

6.3.4   Mooring Line Tension Comparison

6.3.4.1 Mooring Line Mean Tension Comparison

The EPRMS mooring line tension data were recorded at 4 Hz. The numerical simulation of mooring line tensions were sampled at 10 Hz in order to make sure that there were no erroneous snap loads in the simulation.

Overall, the measured tension recorded at the chain-jack agreed reasonably well with the simulated tension (see Fig. 6.5). The difference between the mean tension results from both numerical codes and the field measurement tensions is within 12% in the most tensioned mooring lines. These differences mainly come from the coulomb friction at the fairlead which was combined in the numerical simulation as explained in Chapter 3.

6.3.4.2 Mooring Line Dynamic Tension Comparison

As shown in Fig 6.5 and Table 6.1, the RMS (see equation 6.1) which is the indicator of the mooring line dynamic tension of the most loaded mooring line 1 predicted by both codes were over-predicted by almost 100% than the field measurement during the peak hour of the Hurricane 'Ike' (H_s = 9.3m). The large discrepancy is mainly due to the

friction at the fairlead that significantly reduced the tension after the fairlead roller, especially the dynamic tensions. The measured tension at the chain jack is related to the tension after the fairlead roller while the simulated tension is equal to the tension force before the fairlead. Similar differences were observed in the previous study of Hurricane Isidore ($H_s = 6.4$m). The dynamic mooring line tension was also over-predicted with nearly 100% (Theckumpurath 2006). Also from the comparison of the simulated and measured global motions in Section 6.3.1, it is clear that there exist some differences between the numerical global motion results and the field data. This could also be a reason for the discrepancy in mooring line tensions between the simulation results and field data.

$$RMS = \sqrt{\frac{1}{N}[(X_1 - \mu)^2 + (X_2 - \mu)^2 + \cdots + (X_N - \mu)^2]} \qquad (6.1)$$

where μ is the mean tension; X is the mooring line tensions and N is the number of the mooring line tension samples.
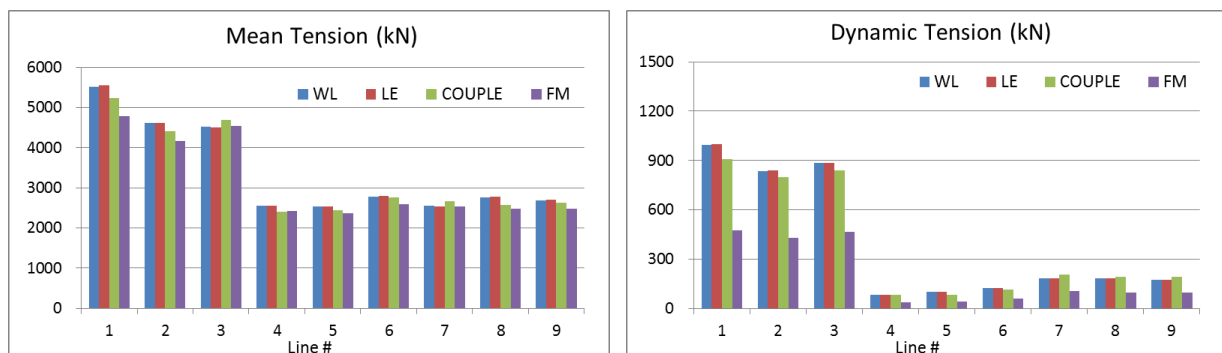

Fig. 6.5 Statistic comparison of mean & dynamic tension during Hurricane 'Ike'.

Table 6.1 Hurricane 'IKE' mooring line tension comparison.

| Mooring Line #	Tension (kN)	WL	LE	COUPLE	FM
Line 1	Max.	8213.29	8254.56	7504.15	6774.64
	Min.	3154.83	3170.69	3202.72	3309.47
	Mean	5521.94	5549.69	5235.55	4793.40
	RMS	996	1001	910	474
Line 2	Max.	6444.32	6471.81	6135.55	5960.61
	Min.	2869.63	2878.27	2741.21	2815.72
	Mean	4614.67	4623.92	4403.73	4164.42
	RMS	836	840	800	431
Line 3	Max.	7138.52	7124.27	6672.33	6476.61
	Min.	3116.08	3025.32	2935.82	3087.06
	Mean	4525.78	4503.26	4692.87	4548.75
	RMS	886	884	837	465
Line 4	Max.	2897.12	2891.34	2757.89	2588.86
	Min.	2614.24	2598.65	2528.83	2259.69
	Mean	2556.47	2548.83	2400.0	2432.3
	RMS	85	85	83	39
Line 5	Max.	2690.27	2713.58	2602.55	2557.72
	Min.	2353.58	2370.17	2316.69	2188.52
	Mean	2529.11	2544.38	2446.52	2367.52
	RMS	99	100	85	40
Line 6	Max.	3015.05	3031.71	3069.27	2851.31
	Min.	2298.85	2310.40	2397.03	2357.55
	Mean	2783.94	2797.931	2757.897	2593.714
	RMS	125	125	116	58
Line 7	Max.	3227.52	3220.68	3158.23	3006.99
	Min.	2065.36	2059.18	2144.04	2055.07
	Mean	2551.62	2543.98	2668.93	2538.91
	RMS	183	182	205	106
Line 8	Max.	3243.28	3269.44	3033.68	2900.24
	Min.	2007.16	2021.32	1912.73	2041.73
	Mean	2754.46	2776.67	2575.52	2479.17
	RMS	182	183	191	94
Line 9	Max.	3214.71	3247.54	3122.65	2873.55
	Min.	2203.67	2221.44	2041.73	2019.49
	Mean	2688.99	2713.42	2624.45	2473.03
	RMS	172	173	191	95

6.4   Winter Storm

'Constitution' experienced a particularly strong winter storm on November 9, 2009. The maximum hourly-average significant wave height, 6.02 m, puts this storm in the category of a 10-year return storm (H_s = 5.4 m), which was also similar in strength to Hurricane Gustav (H_s = 6.4 m) whose path did not come close to 'Constitution'. So it would also be interesting to see the predicted motion and tension results in such a strong winter storm. Using both 'COUPLE' and 'Orcaflex', the author calculated the spar 6DOF motions and mooring line tensions during the peak hour of the storm. Although the met-ocean conditions in this case were not as harsh as in the case of hurricane 'Ike'. The significant wave height (6.02 m) is similar to the significant wave height (6.3 m) in Hurricane 'Isidore' used in the study of Theckumpurath (2006).

6.4.1   Translation Motions Comparison

Fig. 6.6 shows that the statistics of predicted surge, sway and heave using both numerical codes are generally in good agreement with corresponding measurements. The magnitude of the maximum surge motion from the numerical models were 5.6% lower in 'COUPLE' and 12.8% in 'Orcafelx' (WL) and 11.1% in 'Orcaflex' (LE) lower in 'Orcaflex' than the field measurement. The magnitude of the maximum sway motion from numerical models were 4% lower in 'COUPLE' and 9.3% (WL) and 8.3% (LE) lower in 'Orcaflex' than the field data. Similar to the case of hurricane 'Ike', the spar motions in the heave direction were predicted higher than the field measurement (the predicted heave is about 11% higher). This again results from the neglect of the interaction between the TTR and platform in the numerical simulation.
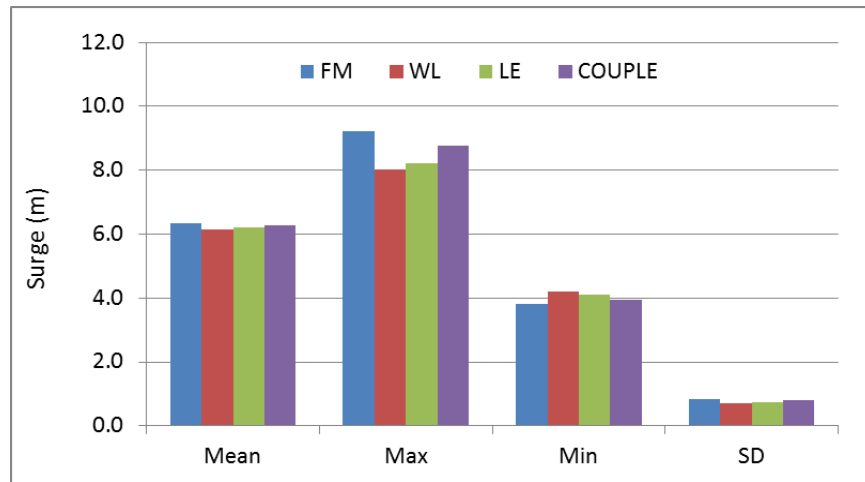
(a) Surge
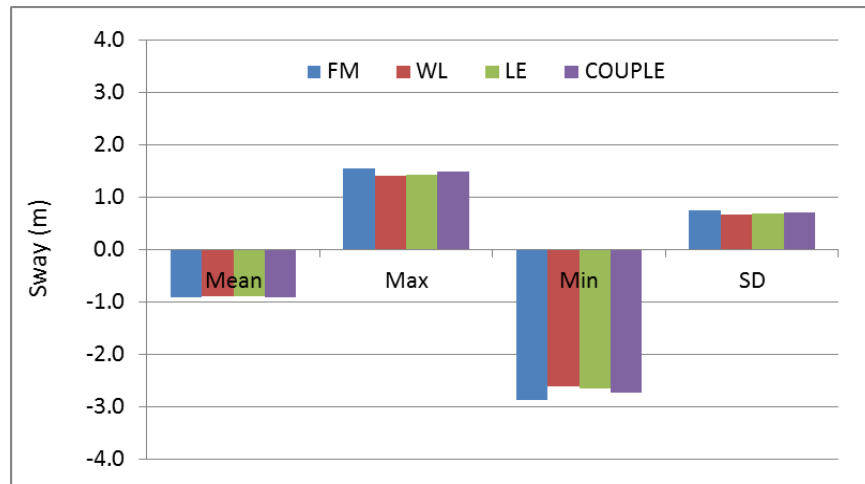
(b) Sway
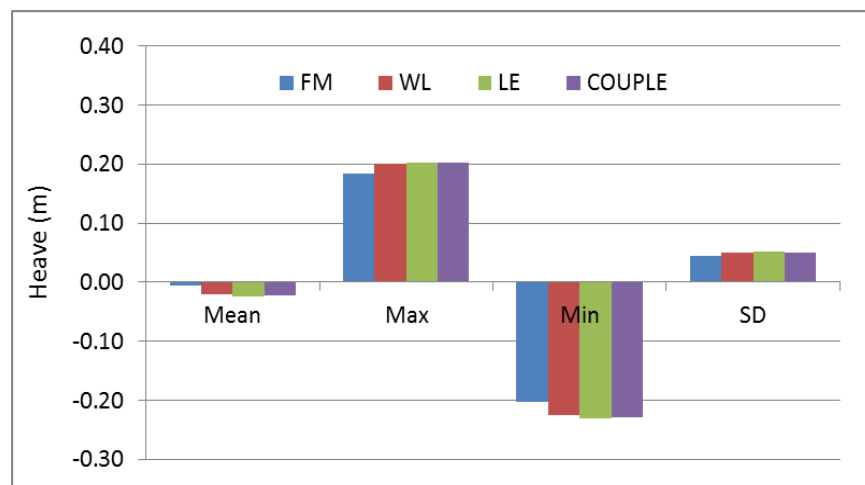
(c) Heave

Fig. 6.6 Comparison of translational motions during winter storm.

(a) roll
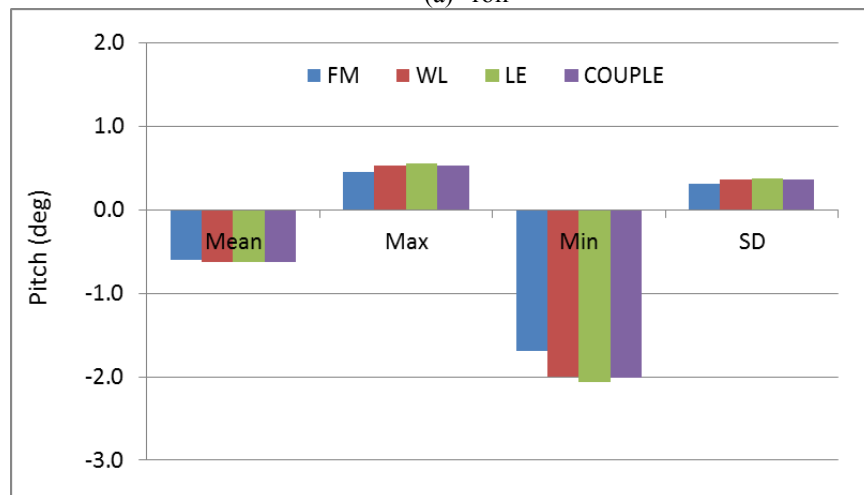
(b) Pitch
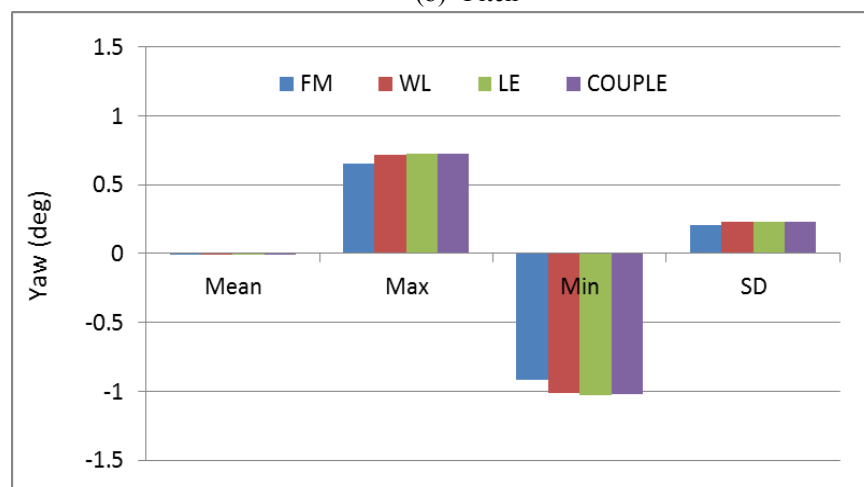
(c) Yaw

Fig. 6.7 Comparison of rotation motion during winter storm.

6.4.2 Rotation Motion Comparison

Similarly, the roll and pitch motions predicted by both 'COUPLE' and 'Orcaflex' were larger than the field measurement. The numerical results are nearly 11% higher given by 'COUPLE', 11.5% by 'Orcaflex' (LE) and 10% by 'Orcaflex' (WL) than the field data in roll while 17% higher by 'COUPLE', 20% by 'Orcaflex' (LE) and 16% by 'Orcaflex' (WL) than field data in the pitch as shown in Fig. 6.7.

Also, from comparing the rotation motions of the spar platform in Hurricane 'Ike' and winter storm, the differences between numerical rotation results and the field measurement data decreased nearly 40% in the case of winter storm. This is mainly because of the decreasing of the intensity and variation of the met-ocean conditions (wind, wave and current). The predicted yaw motions by both numerical codes compared reasonable well with the corresponding measurement from the field data with a maximum difference in 12% in both numerical models due to the coupling effect from the spar roll and pitch motions.
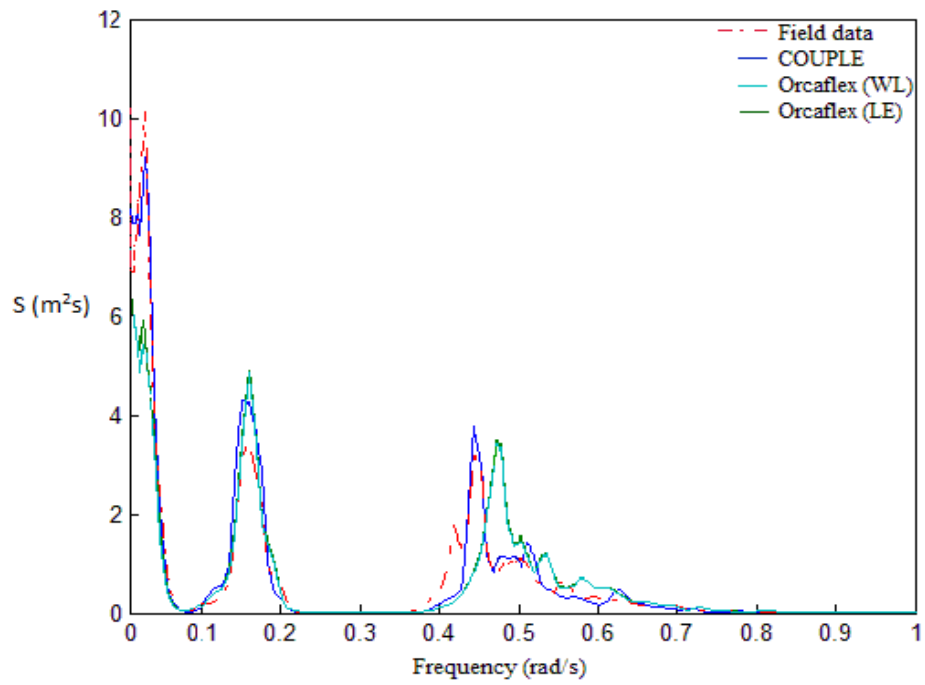
(a) Surge
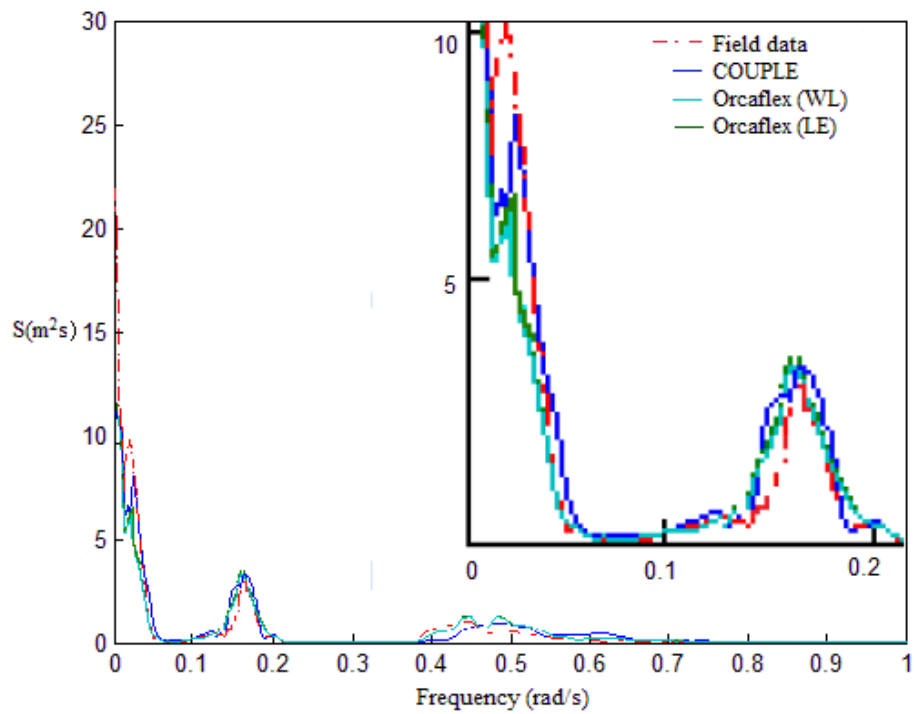
(b) Sway

Fig. 6.8 Comparison of 6DOFs spectra during winter storm.

(a) Heave

(b) Roll

Fig. 6.8 Continued.

(c) Pitch
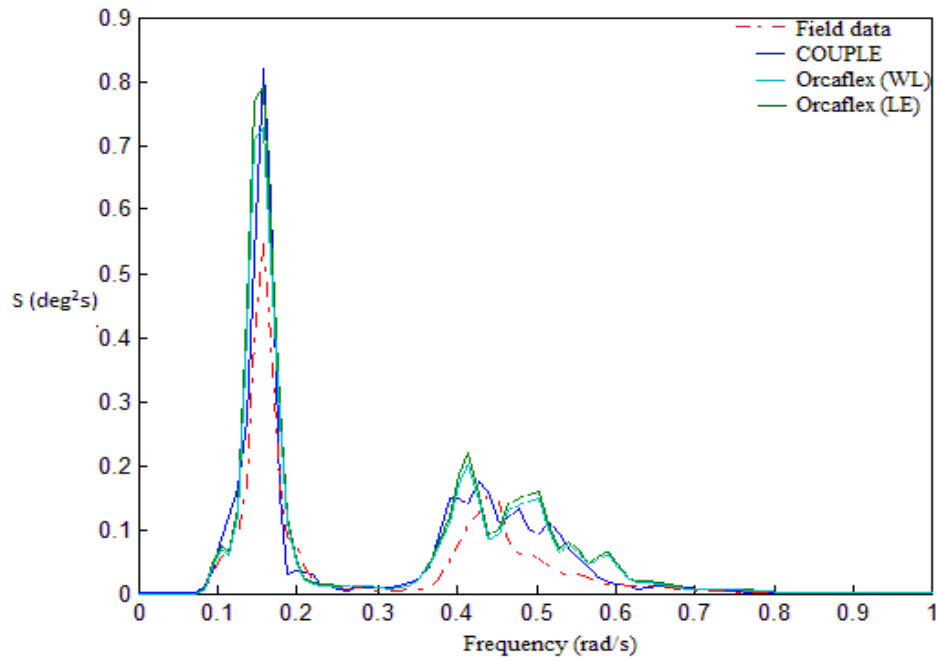
(d) Yaw

Fig. 6.8 Continued.

6.4.3 Power Spectra Comparison

The predicted power spectra of global motion during the peak hour of the winter storm using 'COUPLE' and 'Orcaflex' are compared with the corresponding field measurement in Fig. 6.8.

The observation of the surge and sway spectra shown in Fig. 6.8 indicated that the result from both numerical codes matched with the field measurement near the low-frequency ($\omega = 0 \sim 0.1$ rad/s) and wave frequency range ($\omega = 0.4 \sim 0.6$ rad/s). Also the couplin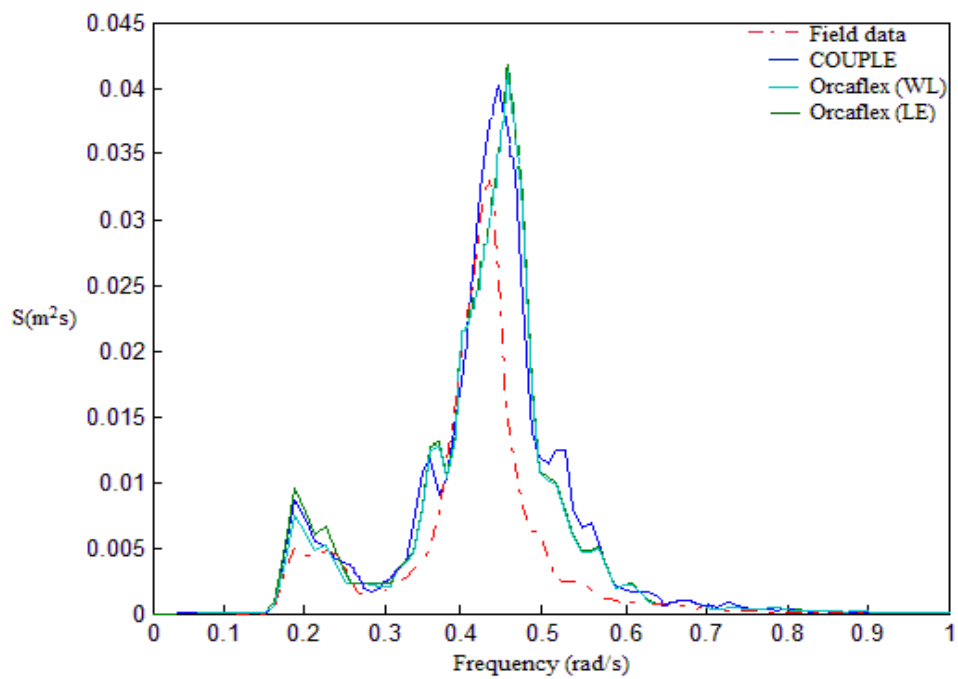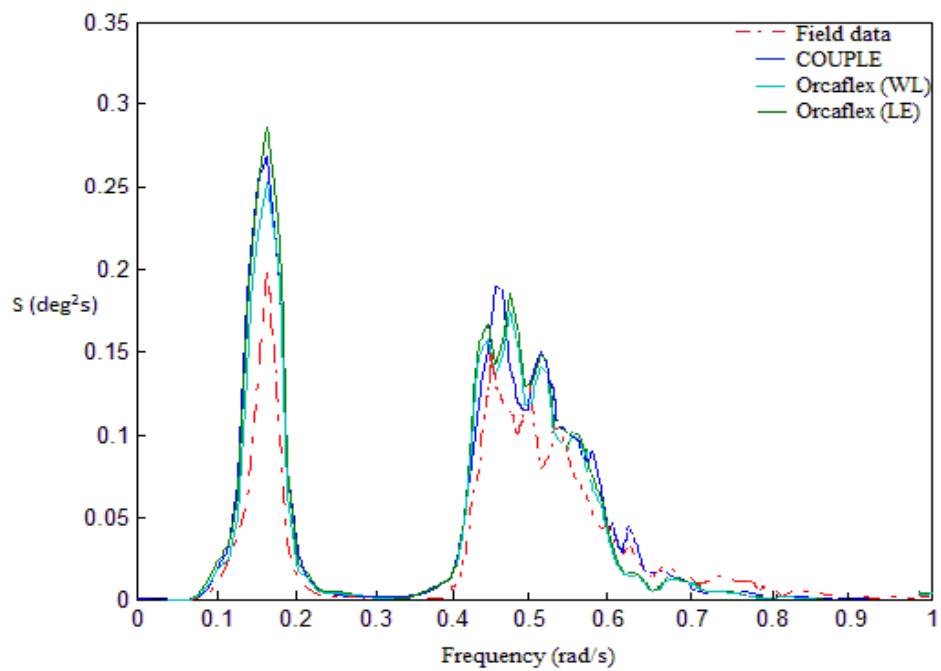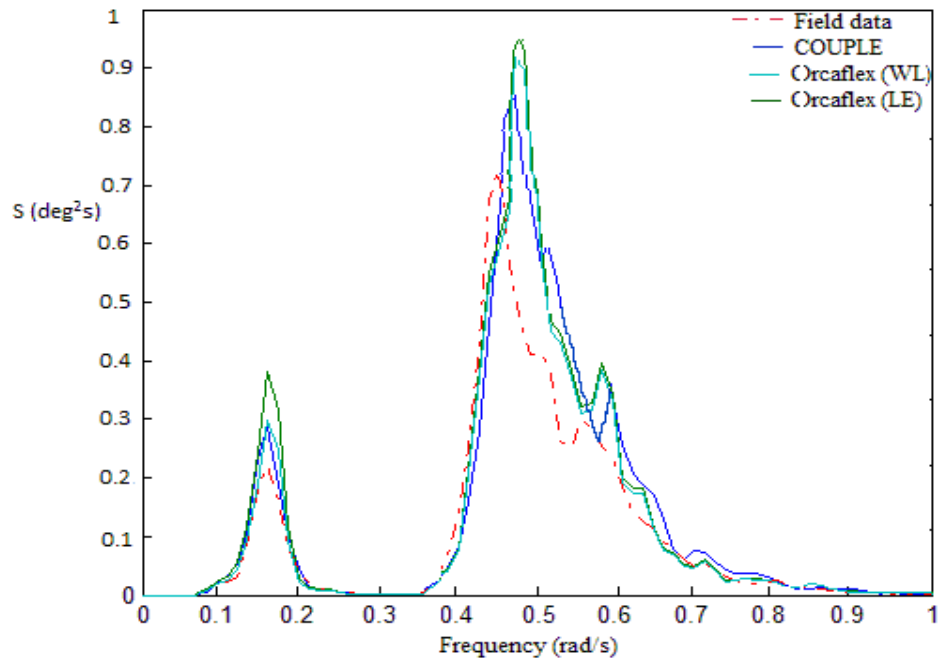g effects on the surge from pitch and roll motion of the platform are also matched in the range at $\omega = 0.1 \sim 0.2$ rad/s. In the low-frequency range, it was found that the energy of the numerical results from 'Orcaflex' (both 'WL' and 'LE') are much smaller than the field measurement while the one from 'COUPLE' matched much better with the field data (also can be found in the statistics result in Section 6.4.1). This discrepancy is mainly due to the modification of LWT used in 'Orcaflex' failed to predict the nonlinear slow drift motion in the low frequency range. Comparing with the hurricane 'Ike' case, the wind speed in the case of winter storm is only 30% of that in Ike while the significant wave height is about 65% in the case of Ike. As a result, the discrepancy between 'Orcaflex' and 'COUPLE' in low-frequency surge motion become more significant as the ratio of the wave induced slow drift motion and wind/current induced slow drift motion increased. It is also necessary to point out that the wave direction in both hurricane 'Ike' (190 deg) and winter storm (160 deg) are both closer to the surge direction. As a result, the discrepancy between the numerical results from 'Orcaflex' and 'COUPLE' in sway direction is not as significant as the ones in surge in both cases.

The numerical results in heave direction matched reasonable well with the field measurement in both low natural and wave frequency with slightly difference due to the missing consideration of the coupling effect from TTR system. Combined with the statistics results, it is clear that the differences between the results from both numerical codes and the field data in heave direction become much smaller than the case of Hurricane 'Ike', this again is mainly due to the decrease of the intensity of wind, current and wave.

The comparison between predicted and measured rotation spectra are shown in the above figure. The predicted roll and pitch by both numerical codes are all larger than the measured spectra in both low frequency and wave frequency range due to the missing consideration of the coupling effect from platform TTR system. It was also found that the energy of yaw numerical motion from both codes are slightly higher than the measurement, which again is due to the effect from the unconsidered TTR in numerical models and its coupling with the pitch and roll motions.

6.4.4   Mooring Line Tension Comparison

Also, the author compared the simulated tensions with the measured tensions during the peak hour of the winter storm. The comparison shows a similar trend as in the case of 'Ike'. The results are compared in Fig. 6.9 and Table 6.2.

6.4.4.1 Mooring Line Mean Tension Comparison

From comparison, the simulated mean tension was within 7% of the measured data for the peak hour of the winter storm for the most loaded mooring line. This difference

results are mainly from the neglect of the friction in the fairlead roller in the simulation. Comparing with the case of hurricane 'Ike', the differences between simulated mean tension and measured mean tension reduced from 12% to 7%. The reduction in the difference between the simulated and measured mean tension can be expected as the intensity of the met-ocean conditions have reduced in wave height, wind and current speed.
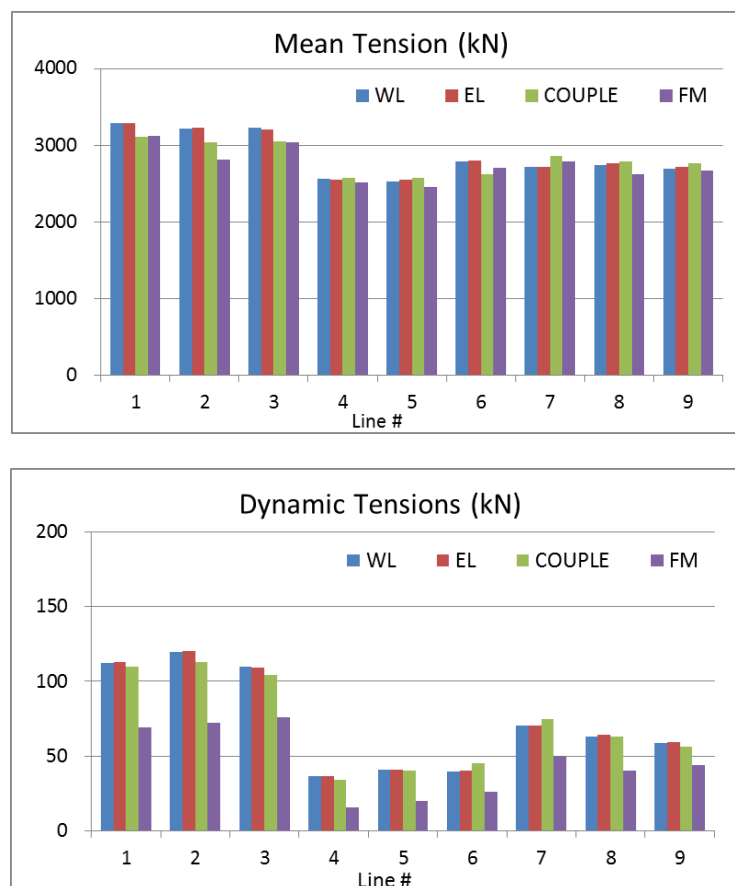

Fig. 6.9 Statistic comparison of mean & dynamic tension during winter storm.

Table 6.2 Winter storm mooring line tension comparison.

Mooring Line #	Tension (kN)	WL	LE	COUPLE	FM
Line 1	Max.	3621.38	3639.57	3533.57	3411.78
	Min.	2962.81	2971.42	2991.06	2851.31
	Mean	3285.87	3292.46	3106.09	3124.90
	RMS	112	113	109	69
Line 2	Max.	3712.70	3727.61	3717.20	3091.51
	Min.	2647.62	2655.59	2359.45	2535.49
	Mean	3218.51	3224.96	3039.54	2808.20
	RMS	120	120	113	72
Line 3	Max.	3534.49	3527.44	3432.87	3318.37
	Min.	2740.63	2757.90	2501.78	2771.24
	Mean	3223.04	3207.00	3048.00	3036.98
	RMS	110	109	104	76
Line 4	Max.	2647.52	2589.59	2642.24	2620.00
	Min.	2492.26	2429.13	2487.28	2459.87
	Mean	2556.48	2548.83	2568.34	2516.12
	RMS	37	36	34	16
Line 5	Max.	2669.64	2691.17	2702.07	2562.18
	Min.	2482.40	2499.90	2520.80	2375.35
	Mean	2529.12	2544.38	2547.43	2449.61
	RMS	41	41	40	20
Line 6	Max.	2872.46	2886.90	2781.35	2846.86
	Min.	2513.96	2526.59	2472.77	2593.31
	Mean	2783.94	2797.93	2622.63	2702.86
	RMS	40	40	45	26
Line 7	Max.	2981.81	2975.86	3299.04	2966.96
	Min.	2422.63	2415.38	2419.30	2571.07
	Mean	2718.84	2713.42	2862.59	2791.50
	RMS	71	70	75	50
Line 8	Max.	2900.29	2932.44	2857.03	2784.59
	Min.	2588.41	2596.66	2548.67	2419.83
	Mean	2744.66	2766.79	2783.70	2626.63
	RMS	63	64	63	40
Line 9	Max.	3073.90	3102.72	2974.00	2842.41
	Min.	2463.68	2481.94	2533.96	2442.07
	Mean	2688.99	2713.42	2759.99	2666.02
	RMS	59	59	56	44

6.4.4.2 Mooring Line Dynamic Tension Comparison

The comparison of the predicted RMS of the 9 mooring lines and the corresponding measured RMS shows that the simulated tensions are much greater than the corresponding measured ones, nearly 100% greater than the measured RMS of the most loaded mooring line, which is similar with the hurricane 'Ike' case. The large difference again is due to the neglect of the friction at the mooring fairlead. The difference in the tensions (both mean and dynamic tensions) between the two codes, 'COUPLE' and 'Orcaflex', are within 10% for the whole peak-hour simulation duration. The comparison of mooring line tensions in the case of Hurricane 'Ike' and winter storm may conclude that the fairlead friction has a significant effect on the mooring line tensions, especially for the dynamic tensions.

6.5   Summary of Differences in 'Orcaflex' and 'COUPLE'

6.5.1   Motions Differences

In this study, the numerical results obtained by 'Orcaflex' were compared with the simulation results from 'COUPLE'. The differences between these two simulated results mainly results from the difference linear and nonlinear wave theories and the mooring numerical scheme they employed because the wind and current simulation in these two codes were identical. As the previous study (Cao and Zhang 1997), the modified linear wave theories, such as WL and LE, cannot accurately predict slow-drift response of the spar platform. The main reason for their inaccuracy is the neglect of interactions among wave components constituting an incident wave field in these empirical models. On the contrary, 'COUPLE' used the HWM which can compute wave kinematics exactly up to

the second order in order to accurate predict the slow drift motion of the structure in the low frequency range. This could explain that the numerical result computed from 'COUPLE' is closer to the field measurement in the low frequency range than the two modification models from 'Orcaflex'. Also with the increase in the contribution of wave induced slow drift motion in the low frequency range, the discrepancy of the simulated motions between these two codes became more and more significant.

6.5.2   Mooring Line Tension Differences

'Orcaflex' is a commercial code developed by Orcina (2000) which employs a finite difference method. The mass of each element is lumped at its center. On the other hand, 'COUPLE' used finite element method (see chapter 2) to simulate the mooring line and solve the partial differential equation of the mooring line motion equations. As a result, there exists some difference in the tension results obtained by 'COUPLE' and 'Orcaflex'. However, the biggest difference between the numerical results in the most loaded mooring line is within 10% in magnitude which could confirm a good agreement between these two codes. It is also necessary to point out that the numerical motion results of the platform from these two numerical codes were not identical which could also impact the mooring results as the platform and the mooring system were coupled together in both the numerical codes.

7   CONCLUSION

The numerical simulation of a truss spar, named 'Constitution', interacting with its mooring line/SCR system under the impact of severe storms, was performed using an in-house numerical code 'COUPLE' and a commercial code 'Orcaflex', respectively. The simulated results of the 6 DOF motion of the spar and its mooring line tensions obtained using the two numerical codes were then compared with each other and the field measurement, for the cases during the peak hour of Hurricane 'Ike' occurred on September 12th of 2008 and a strong winter storm on November the 9th of 2009.

Since the wind coefficients obtained from the related wind-tunnel tests were not available to us, the related wind coefficients of the spar platform were estimated based on the field measurements of the mean surge and sway in the selected hours when winds were strong and waves and currents are relatively weak. The wave loads on the spar hull were computed using the Morrison equation in both numerical codes. While the wave kinematics was calculated based on the nonlinear HWM in 'COUPLE', that was calculated using two modifications of LWT (wheeler stretching and linear extrapolation) in 'Orcaflex'. Overall, the numerical results from both codes show a reasonable agreement with the related field measurements of 6 DOF motions. The main differences in prediction the global motions result from the use of the modified LWT in 'Orcaflex' and the nonlinear HWM in 'COUPLE', which were observed in the predicted slow-drift motion. The comparison of the related statistics and energy spectra of spar motions shows that the modified LWT employed in 'Orcaflex' fails to predict the slow-drift motion (in the low-frequency range) accurately, which is crucial to the station-keeping and the safety of the

offshore structures. It has been shown that with the increase in the contribution from the wave-induced slow-drift motion this discrepancy becomes more substantial. Because the configuration of the TTR system of the spar is not available to us, the forces of the TTR system on the spar were approximated and simplified as a steady force based on the field measurement of each TTR mean tension. However, it was found that this simplification might cause significant errors in the simulated heave, roll and pitch of the spar.

Similar to the trends observed in the comparison of the spar global motions, the simulated mean tension in mooring lines using the two numerical codes also matched well with the related field measurement. However, the simulated dynamic tensions by either numerical code were much greater than the related field measurements. It is because that the friction at fairlead rollers was not accounted in the numerical simulation. The reduction of the friction at fairlead rollers in measured dynamic tensions is extremely difficult if not impossible to estimate considering that the friction coefficients at each fairlead roller may vary significantly depending on factors ranging from the installation to marine corrosion.

This study concludes that the use of Morison equation together with the nonlinear HWM is adequate to predict the response of a spar under the impact of severe storms. However, using the modifications of linear wave theory together with the Morison equation may not accurately predict the slow-drift motion. The modeling of the coupling effect from the TTR system and the determining the friction coefficients at the fairlead rollers are the challenges of the future research.

REFERENCES

API 2INT- MET, 2007. Guidance on Hurricane Conditions in Gulf of Mexico. American Petroleum Institute, Washington, DC.

API RP2SK, 1996. Recommended Practice for Design and Analysis of Station keeping Systems for Floating Structures. American Petroleum Institute, Washington, DC.

Cao, P.M., Zhang, J., 1997. Slow motion responses of compliant offshore structures. International Journal of Offshore and Polar Engineering 7(2), 119-126.

Chen, X., Ding, Y., Zhang, J., Liagre, P., Niedzwecki, J., Teigen, P., 2006. Coupled dynamic analysis of a mini TLP: comparison with measurements. Ocean Engineering 33 (1), 93-117.

Garrett, D.L., 1982. Dynamic analysis of slender rods. Journal of Energy Resources Technology, 104, 302-307.

Http://www.gomr.boemre.gov/homepg/offshore/deepwatr/dpstruct.html. Bureau of Ocean Energy Management, Regulation and Enforcement (BOEMRE), accessed on March 2nd, 2012.

Kiecke, A., Zhang, J., 2012. Estimate of mooring line damage accrued by a GOM truss spar based on field measurements. International Offshore and Polar Engineering Conference, Maui, HI.

Kim, M.H., Chen, W., 1994. Slender-body approximation for slowly-varying wave loads in multi-direction waves. In: Proceedings of the 6th Offshore and Polar Engineering Conference, Los Angeles, CA.

Kim, M.H., Koo, B.J., Mercier, R.M., Ward, E.G., 2005. Vessel/mooring/riser coupled dynamic analysis of a turret-moored FPSO compared with OTRC experiment. Ocean Engineering 32, 1780-1802.

Love, A., 1944. A Treatise on the Mathematical Theory of Elasticity. 4th Edition, Dover Publications, NY.

Ma, W., Lee, M.Y., Zou, J., Huang, E., 2000. Deepwater nonlinear coupled analysis tool. In: Proceedings of the Offshore Technology Conference, Houston, TX, OTC 12085.

Ma, W., Webster, W.C., 1994. An Analytical Approach to Cable Dynamics: Theory and User Manual. SEA GRANT PROJECT R/OE-26. Department of Naval Architecture and Offshore Engineering, University of California at Berkeley, September 1994.

Magee A., Sablock A., Maher J., Halkyard J., Finn L., Dutta Indra., 2000. Heave plate effectiveness in the performance of the truss spar. In: Proceedings of the ETCE/OMAE2000 Joint Conference on Energy for the New Millennium, New Orleans, LA.

Morison, J.R., O'Brien, M.P., Johonson, J.W. and Shaaf, S.A., 1950. The forces exerted by surface waves on plies. Petrol. Trans. AIME 189, 149-154.

Newman, J.N., 1974. Second order slowly varying forces on vessels in irregular waves. In: Symposium On Dynamic of Marine Vehicles and Structures in Waves, London, UK.

Nordgren, R, 1974. On computation of the motion of elastic rods. ASME Journal of Applied Mechanics, September, 777-780.

Orcina, Ltd., Orcaflex User Manual, 1987-2010.

Ormberg, H., Larsen, K., 1997. Coupled analysis of floating motion and mooring dynamics for a turret moored tanker. In: Proceedings of the Behavior of Offshore Structures Conference (BOSS), Delft, The Netherlands.

Ormberg, H., Sodahl, N., Steinkjer, O., 1998. Efficient analysis of mooring systems using de-couple and coupled analysis. In: Proceedings of the 17th International Conference on Ocean, Offshore and Arctic Engineering, Lisbon, Portugal.

Pauling, J.R., Webster, W.C., 1986. A consistent, large-amplitude analysis of the coupled response of a TLP and tendon system. In: Proceeding 5th International Mechanics and Arctic Engineering Symposium, Tokyo, Japan.

Pinkster, J.A., 1980. Low frequency second-order wave exciting forces on floating structures. Ph.D thesis, Report 650, Maritime Research Institute Netherlands (NSMB).

Prislin, I., R. Rainford, S. Perryman and R. Schilling, 2005. Use of field monitored data for improvement of existing and future offshore facilities. SNAME Paper D5.

Ran, Z., Kim, M.H., 1997. Nonlinear coupled responses of a tethered spar platform in waves. International Journal of Offshore and Polar Engineering 7 (2), 111-118.

Ran, Z., Kim, M.H., Zheng, W., 1998. Copled dynamic analysis of a moored spar in random waves and currents (time-domain vs frequency-domain analysis). In: Proceedings of the 17th International Conference on Ocean, Offshore and Arctic Engineering, Lisbon, Portugal.

Rodenbusch, G., and Forristall, G.Z., 1986. An empirical for random directional wave kinematics near the free surface. In: Proceedings of the 18th Annual Offshore Technology Conference, Houston, TX.

Spell, C.A., Zhang, J., Randall, R.E., 1995. Hybrid wave model for unidirectional irregular waves, Part II. Comparison with Laboratory Measurements. Journal of Applied Ocean Research 18, 93-110.

Tahar, A., Finn, L., Liagre, P., Halkyard, J., 2005. Full scale data comparison for 'Horn Mountain' spar mooring line tensions during hurricane isidore. In: Proceedings of the 24th International Conference on Offshore Mechanics and Arctic Engineering, Athens, Greece.

Theckumpurath, B., 2006. Numerical simulation of the truss spar 'Horn Mountain'. MS Thesis, Ocean Engineering Program, Civil Engineering Department, Texas A&M University.

Wheeler, J.D., 1970. Method for calculating forces produced by irregular waves. Journal of Petroleum Technology, March, 119-113.

Yang, M., Teng, B., Ning, D., Shi, Z., 2011. Coupled dynamic analysis for wave interaction with a truss spar and its mooring line/riser system in time domain. Ocean Engineering 39, 72-87.

Zhang, J., Randall, R., Spell, C., 1991. On wave kinematics approximate method. In: Proceedings of the 23rd Annual Offshore Technology Conference, Houston, TX.

Zhang, J., Yang, J., Wen, J., Prislin, I., Hong, K., 1996. Hybrid wave model for unidirectional irregular waves part I. theory and numerical scheme. Journal of Applied Ocean Research 18, 77-92.

APPENDIX A

North side

Platform Topside Section (Looking North)	Project Area (m^2)	Geometry Center Height (m)
1A: Spar Hard Tank	455.2	7.6
1B: Spar-deck to Sub-Cellar Deck	142.3	17.6
1C: Sun-Cellar-Deck to Production-Deck	112.4	24.7
2: Cellar-Deck to Production-Deck	442.2	32.8
3: Production-Deck to Main-Deck	416.9	43.1
4: West Stairs	63.2	37.8
5: East Stairs	63.2	37.8
6: Permanent Quarter	298.4	54.8
Total Area (m^2) and Pressure Center (m)	2029.7	30.7

East side

Platform Topside Section (Looking East)	Project Area (m^2)	Geometry Center Height (m)
1A: Spar Hard Tank	455.2	7.6
1B: Spar-deck to Sub-Cellar Deck	142.3	19.4
1C: Sun-Cellar-Deck to Production-Deck	112.4	24.7
B: Cellar-Deck to Production-Deck	611.3	32.8
C: Production-Deck to Main-Deck	576.4	43.1
D: Spar Stairs	63.2	37.8
E: Flare Boom	253.6	63.4
Total Area (m^2) and Pressure Center (m)	2267.0	31.9

VITA

Name: Chengxi LI

Address: Zachry Department of Civil Engineering

                     Texas A&M University

                     3136 TAMU

                     College Station, TX, 77843-3136

Email Address: lichengxi11@gmail.com

Education: B.E., Naval Architecture & Ocean Engineering

                       Tianjin University, 2010

                       M.S., Ocean Engineering

                       Texas A&M University, 2012